Stochastic-Strength-Based Damage Simulation Tool for Ceramic Matrix and Polymer Matrix Composite Structures

Noel N. Nemeth, Brett A. Bednarcyk, and Evan J. Pineda
Glenn Research Center, Cleveland, Ohio

Owen J. Walton
University of Wisconsin–Madison, Madison, Wisconsin

Steven M. Arnold
Glenn Research Center, Cleveland, Ohio

NASA STI Program . . . in Profile

Since its founding, NASA has been dedicated to the advancement of aeronautics and space science. The NASA Scientific and Technical Information (STI) Program plays a key part in helping NASA maintain this important role.

The NASA STI Program operates under the auspices of the Agency Chief Information Officer. It collects, organizes, provides for archiving, and disseminates NASA's STI. The NASA STI Program provides access to the NASA Technical Report Server—Registered (NTRS Reg) and NASA Technical Report Server— Public (NTRS) thus providing one of the largest collections of aeronautical and space science STI in the world. Results are published in both non-NASA channels and by NASA in the NASA STI Report Series, which includes the following report types:

- TECHNICAL PUBLICATION. Reports of completed research or a major significant phase of research that present the results of NASA programs and include extensive data or theoretical analysis. Includes compilations of significant scientific and technical data and information deemed to be of continuing reference value. NASA counter-part of peer-reviewed formal professional papers, but has less stringent limitations on manuscript length and extent of graphic presentations.

- TECHNICAL MEMORANDUM. Scientific and technical findings that are preliminary or of specialized interest, e.g., "quick-release" reports, working papers, and bibliographies that contain minimal annotation. Does not contain extensive analysis.

- CONTRACTOR REPORT. Scientific and technical findings by NASA-sponsored contractors and grantees.

- CONFERENCE PUBLICATION. Collected papers from scientific and technical conferences, symposia, seminars, or other meetings sponsored or co-sponsored by NASA.

- SPECIAL PUBLICATION. Scientific, technical, or historical information from NASA programs, projects, and missions, often concerned with subjects having substantial public interest.

- TECHNICAL TRANSLATION. English-language translations of foreign scientific and technical material pertinent to NASA's mission.

For more information about the NASA STI program, see the following:

- Access the NASA STI program home page at http://www.sti.nasa.gov

- E-mail your question to help@sti.nasa.gov

- Fax your question to the NASA STI Information Desk at 757-864-6500

- Telephone the NASA STI Information Desk at 757-864-9658

- Write to:
  NASA STI Program
  Mail Stop 148
  NASA Langley Research Center
  Hampton, VA 23681-2199

Stochastic-Strength-Based Damage Simulation Tool for Ceramic Matrix and Polymer Matrix Composite Structures

Noel N. Nemeth, Brett A. Bednarcyk, and Evan J. Pineda
Glenn Research Center, Cleveland, Ohio

Owen J. Walton
University of Wisconsin–Madison, Madison, Wisconsin

Steven M. Arnold
Glenn Research Center, Cleveland, Ohio

National Aeronautics and
Space Administration

Glenn Research Center
Cleveland, Ohio 44135

October 2016

Acknowledgments

Level of Review: This material has been technically reviewed by technical management.

Available from

Stochastic-Strength-Based Damage Simulation Tool for Ceramic Matrix and Polymer Matrix Composite Structures

Noel N. Nemeth, Brett A. Bednarcyk, and Evan J. Pineda
National Aeronautics and Space Administration
Glenn Research Center
Cleveland, Ohio 44135

Owen J. Walton[1]
University of Wisconsin–Madison
Madison, Wisconsin 53706

Steven M. Arnold
National Aeronautics and Space Administration
Glenn Research Center
Cleveland, Ohio 44135

Summary

Stochastic-based, discrete-event progressive damage simulations of ceramic-matrix composite and polymer matrix composite material structures have been enabled through the development of a unique multiscale modeling tool. This effort involves coupling three independently developed software programs: (1) the Micromechanics Analysis Code with Generalized Method of Cells (MAC/GMC), (2) the Ceramics Analysis and Reliability Evaluation of Structures Life Prediction Program (CARES/ *Life*), and (3) the Abaqus finite element analysis (FEA) program. MAC/GMC contributes multiscale modeling capabilities and micromechanics relations to determine stresses and deformations at the microscale of the composite material repeating unit cell (RUC). CARES/*Life* contributes statistical multiaxial failure criteria that can be applied to the individual brittle-material constituents of the RUC. Abaqus is used at the global scale to model the overall composite structure. An Abaqus user-defined material (UMAT) interface, referred to here as "FEAMAC/CARES," was developed that enables MAC/GMC and CARES/*Life* to operate seamlessly with the Abaqus FEA code.

For each FEAMAC/CARES simulation trial, the stochastic nature of brittle material strength results in random, discrete damage events, which incrementally progress and lead to ultimate structural failure. This report describes the FEAMAC/CARES methodology and discusses examples that illustrate the performance of the tool. A comprehensive example problem, simulating the progressive damage of laminated ceramic matrix composites under various off-axis loading conditions and including a double-notched tensile specimen geometry, is described in a separate report.

1.0   Introduction

A software tool has been developed that simulates the stochastic-based, discrete-event progressive damage of composite material structures. This tool, called the Finite Element Analysis—Micromechanics Analysis Code/Ceramics Analysis and Reliability Evaluation of Structures (FEAMAC/CARES), is a unique multiscale modeling tool that was developed to simulate how damage initiates and develops in ceramic matrix composite (CMC) structures under thermomechanical loading. It involves micromechanics to determine stresses and deformations at the microscale of the repeating unit cell (RUC) of the composite material and stochastic-strength-based multiaxial failure criteria that can be applied to

---

[1]Undergraduate Student Research Program (USRP) Fall 2010 Intern, Life Prediction Branch, Glenn Research Center, and University of Wisconsin–Madison.

the individual brittle-material constituents of the RUC to simulate the development of damage. Because the technology is generic, it is also applicable to other composite material systems, such as polymer matrix composite (PMC) materials, provided that the composite's individual material constituents act in a brittle-like manner.

The need for materials that can withstand very high temperatures and harsh environments has been motivating the development of fiber-reinforced CMCs. These CMCs will be used in turbine hot-section components (e.g., blades, vanes, combustor liners, and nozzles), the airframe leading edges for hypersonic vehicles, and the fuel cladding tubes (fuel rods) in nuclear reactors. CMCs, which have higher use temperatures and lower densities than their metallic counterparts, enable (in the case of turbine components) a reduction in engine thrust specific fuel consumption. CMCs display complex failure behaviors that are influenced by the specific arrangement and bonding of the separate ceramic material constituents. Because of this, there is a clear need to develop and improve models of this synergistic failure process so that components can be designed for assured safety, efficiency, life, performance, and cost.

CMCs also have high fracture toughness and impact resistance compared with monolithic ceramic parts. They display gradual (graceful) failure mechanisms characterized by damage accumulation through distributed microcracking prior to ultimate failure. Conversely, monolithic ceramics are brittle and will shatter suddenly and catastrophically at a critical load. Monolithic ceramics are best suited for applications involving small, stubby, or thick parts, whereas CMCs are more appropriate for larger parts, where greater surface-to-volume ratios are required and the ability to tolerate some damage and not fail catastrophically is essential.

There is much literature available regarding CMC behavior and modeling. Curtin (2000) and Ramamurty et al. (2000) provide a good overview of this topic, and Miller et al. (2006) reviews the durability and life prediction models available for CMCs at the time. CMCs typically consist of three major components: fibers, matrix, and an interface material that separates each fiber from the matrix. The interface material coats the fiber and provides a buffer for crack deflection through both debonding between the fiber and matrix and energy dissipation through frictional sliding (Evans, 1995). The interface material is designed to prevent cracks that are propagating in the matrix from penetrating and rupturing the embedded fibers, allowing fibers to bridge matrix cracks and make crack propagation more difficult. However, this process gradually degrades component stiffness, although the component can still remain intact—held together by the undamaged fibers. CMCs are thus able to exhibit nonlinear macroscopic deformation because of the redistribution of stresses that follows repeated matrix cracking events throughout the material volume. Failure of the part occurs when all of the fibers have ruptured or when complete loss of stiffness (in the case of flexural loading) occurs.

At the microscale of the composite RUC (the periodic arrangement of the heterogeneous microstructure—fiber, matrix, and interface—that repeats itself to generate the overall microstructure), the CMC can be regarded as a structure consisting of various monolithic ceramic constituents. Understanding the behavior of the individual material constituents and their bimaterial interfaces provides the basis for understanding the macroscopic behavior of the composite. The damage process in CMCs is stochastic because the composite's individual brittle material constituents and their bimaterial interfaces vary in strength because of numerous features that are formed during processing. These include flaws of various sizes, shapes, and orientations. Other sources of randomness that contribute to the stochastic nature of the damage response include variations within fiber tows (such as fiber clustering, fiber alignment, and fiber interface coating uniformity), variations outside the fiber tow (such as undulations and nesting in multilayer fabrics), and the presence of large-scale voids resulting from incomplete infiltration of matrix material into the composite preform.

The objective of this report is to describe a new integrated modeling tool that is coupled with commercial finite element analysis (FEA) software to simulate the stochastic nature of damage initiation and subsequent propagation in CMCs. It can also be used so simulate damage in PMC material systems, provided that the individual constituents collectively act in a brittle-like manner. This development effort involved the coupling of three independently developed software programs: (1) the Micromechanics Analysis Code with Generalized Method of Cells (MAC/GMC) (Bednarcyk and Arnold, 2002a, 2002b),

(2) the Ceramics Analysis and Reliability Evaluation of Structures Life Prediction Program (CARES/*Life*) (Nemeth et al., 2003, 2005), and (3) the Abaqus FEA program (Dassault Systèmes Simulia Corp., 2011).

MAC/GMC is a micromechanics-based code that operates at the constituent (i.e., fiber, matrix, and interface) level of the composite material. It provides multiscale modeling capabilities and micromechanics relations to homogenize and localize the composite layup, while also determining stresses and deformations at every scale of the composite material. CARES/*Life* provides stochastic-strength-based multiaxial failure criteria that can be applied to the individual brittle-material constituents of the RUC. Abaqus is used to model the overall composite structure. The fully coupled, multiscale code, referred to here as "FEAMAC/CARES," enables MAC/GMC and CARES/*Life* to operate interactively with the Abaqus FEA code through the Abaqus user-defined material (UMAT) interface. For each FEAMAC/ CARES simulation trial, the stochastic nature of brittle material strength results in random discrete microcracking events that progress incrementally and lead to ultimate structural failure. The effects of bimaterial interfaces and frictional sliding are not considered here and are left for future work.

2.0 Overview of CARES/*Life*, MAC/GMC, and FEAMAC

2.1 CARES/*Life*

CARES/*Life* software is used for the strength and life prediction aspect of this investigation. The software was originally developed to predict the probability of failure of full-scale monolithic (non-fiber-reinforced) ceramic components under thermomechanical loading over a service time (Nemeth et al., 2003, 2005; Connecticut Reserve Technologies, 2015). Because ceramic materials typically exhibit large amounts of scatter in strength, CARES/*Life* uses Weibull-based probabilistic models to describe ceramic failure strength. It functions as a postprocessor to commercial FEA software packages, which predict the needed stress distribution of the component. In this report the core CARES/*Life* reliability calculation algorithms have been modified to operate at the RUC level of a composite to predict the failure of the individual brittle constituents: the fiber, matrix, and interface. These material constituents are themselves monolithic ceramics and are thus ideal for analysis with the CARES/*Life* reliability models.

CARES/*Life* can predict the probability of failure for fast fracture, which is the risk that a component will fail catastrophically from preexisting flaws (which are present inherently from processing). CARES/*Life* also considers how strength degrades over time and cyclic loading from subcritical crack growth (SCG), which is the progressive extension of a crack over time under loading. SCG typically causes a flaw to extend until a critical length or damage level is reached that results in catastrophic failure. CARES/*Life* can consider the effects of multiaxial stress states and can handle multiple time-step loading in a fully transient and generalized manner.

2.2 MAC/GMC

The MAC/GMC software models the RUC of the composite material to predict the homogenized, macroscopic thermomechanical material response under generalized loading conditions (Bednarcyk and Arnold, 2002a, 2002b; Aboudi et al., 2013) as well as the local fields in the constituents. It uses the GMC (Paley and Aboudi, 1992; Aboudi et al., 2013) micromechanics theory and has many different material constitutive models that can represent a large number of material types and RUC configurations. A key advantage of the GMC is that it is computationally much faster than an analysis using a finite element model of the RUC, although a tradeoff is involved with the level of detail and accuracy that can be obtained for the stress fields in the RUC. This speed advantage becomes critical when a multiscale analysis with a finite element model of a composite structure requires lengthy run times. An improved version of GMC called high-fidelity GMC, or HFGMC, has also been developed (Aboudi et al., 2013). In comparison to GMC, HFGMC offers greater accuracy and detail in the local stress fields of the RUC but at the cost of greater computational overhead and slower computation speed. In this report we only discuss results using GMC.
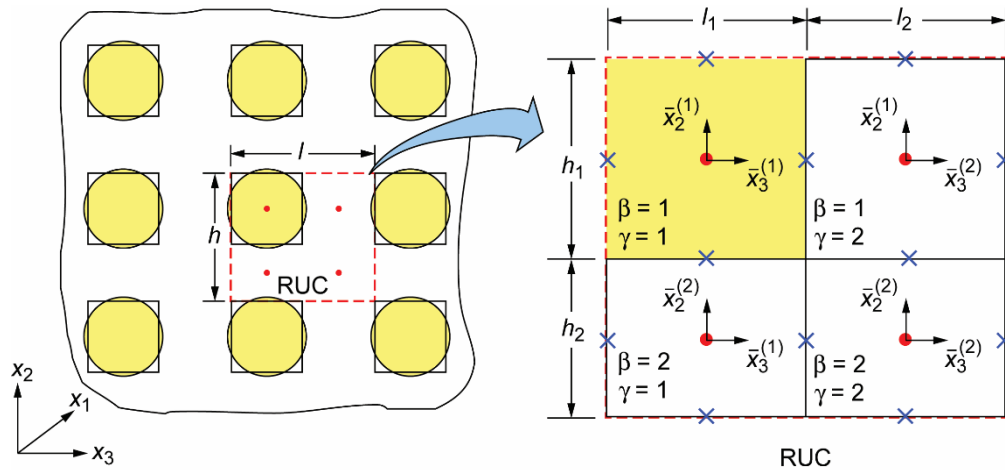
Figure 1.—Two-dimensional, square-packed example of a fiber-in-matrix repeating unit cell (RUC). Local subcell stress fields are centroidal values in the GMC methodology.

The GMC model breaks down the composite RUC into subdomains or subcells. Figure 1 shows this schematically. The centroids of the subcells (as indicated in the figure) are an important feature in the GMC methodology. The rectangular shape denoting the subcell indicates the region of influence of the subcell's centroid; the local stress and strain field associated with the centroid is calculated.

2.3 FEAMAC

FEAMAC (Bednarcyk and Arnold, 2006) is a multiscale modeling tool that couples the Abaqus FEA software package with the MAC/GMC 4.0 composite analysis software package. With FEAMAC, Abaqus can call MAC/GMC 4.0 to determine the homogenized macroscopic material response at the integration points within the elements composing the structural FEA model. In essence, MAC/GMC 4.0 operates as a nonlinear constitutive model within Abaqus, representing a heterogeneous composite material. A synergistic approach is employed that executes concurrent multiscaling in time but two-way hierarchical multiscaling in space (Sullivan and Arnold, 2011).

FEAMAC consists of four Abaqus standard user-defined subroutines (Dassault Systèmes Simulia Corp., 2011), as well as six subroutines exclusive to the FEAMAC package (see Fig. 2).

The Abaqus UMAT subroutine provides the strains, strain increments, and current values of state variables at a given finite element material point to MAC/GMC through the front-end subroutine FEAMAC. These strains represent RUC-level strains within MAC/GMC. They are used to calculate local fields within the RUC, any local damage or nonlinearity, and a new, homogenized stiffness and stress state. These are returned to Abaqus, along with the updated state variable. Bednarcyk and Arnold (2006) provides further details on the FEAMAC software implementation.
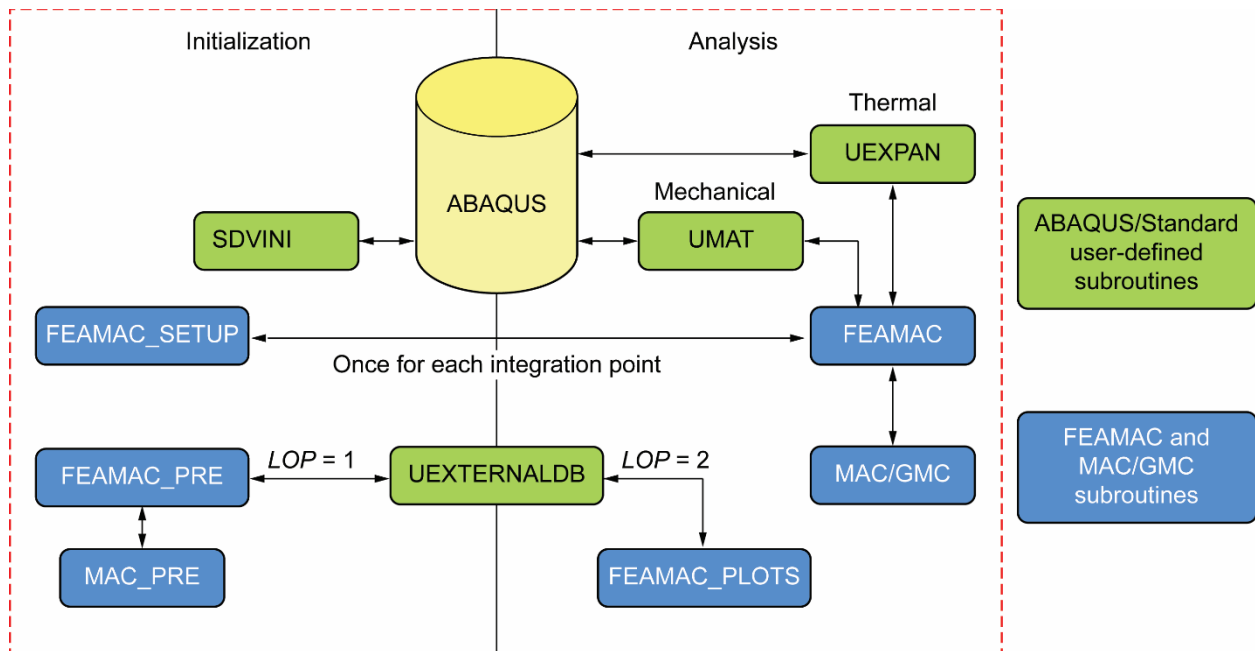
Figure 2.—Software implementation schematic of multiscale operation with FEAMAC. *LOP*1 indicates that subroutine UEXTERNALDB is being called at the start of the current analysis increment, and *LOP*2 indicates that subroutine UEXTERNALDB is being called at the end of the current analysis increment. Subroutines are explained in Pineda et al. (2009) and Dassault Systèmes Simulia Corp. (2011).

3.0   FEAMAC/CARES Implementation

The CARES/*Life* and MAC/GMC codes were both developed in-house at the NASA Glenn Research Center. MAC/GMC was originally developed for metal matrix composites (MMCs) and PMCs to predict their thermomechanical and damage response. For CMCs, MAC/GMC 4.0 lacks well-developed, stochastic life-prediction methodologies appropriate for brittle materials. Conversely, CARES/*Life* was specifically developed to predict the failure potential of monolithic ceramic structures (originally intended for the analysis of small gas turbine hot-section parts) under generalized loading.

CARES/*Life* is, at its essence, a stochastic-based failure criterion algorithm for unreinforced brittle materials that experience multiaxial loading. By treating the RUC itself as structure—consisting of separate monolithic material constituents, CARES/*Life* can be used to assess the failure potential of the RUC constituents. This is possible when CARES/*Life* is used with MAC/GMC because MAC/GMC provides the RUC stress fields (at the local subcell level) and temperature necessary for analysis with CARES/*Life*. Therefore it was advantageous and efficient to integrate the already developed CARES/*Life* algorithm as a failure criterion within MAC/GMC to predict the failure response for the individual brittle material constituents of the RUC. This synergy leverages the unique and mutually exclusive capabilities of both programs. The resulting software coupling is referred to as "FEAMAC/CARES."

The literature reports previous cases where the individual brittle material constituents of a CMC have been treated as isotropic, Weibull-distribution-behaved materials (e.g., Curtin, 1991, 1993; Ahn and Curtin, 1997; Guillaumat and Lamon, 1996; Lamon et al., 1998). The Weibull distribution assumes that the material imperfections where failure could initiate are embedded in a continuous medium, that these flaws do not interact with each other (are isolated from each other), and that the flaw size is small relative to any stress gradients so that the applied stress across the flaw's crack length is negligible. For a flaw embedded in the matrix material of a CMC this is not necessarily true. The flaw may be on the length scale of the fiber diameter (or significantly larger) and stress gradients along the flaw length may exist because of the interaction of the constituent materials in the RUC. Accounting for stress gradients along the crack length is more complicated and results in non-Weibull strength distributions (Brueckner-Foit et al., 2000).

Matrix flaws that are as large, or larger, than the RUC are also inconsistent with the assumptions behind the Weibull strength distribution. In that case the material constituents cannot be treated as separate continuum materials, instead the flaw would have to be modeled explicitly. However, because we assume that the RUC is periodic (an infinitely repeating pattern), the collective effect of the periodic stress distribution (across all the RUCs) will have an effect at the macroscale analogous to that postulated by composite failure theories such as the Puck multiaxial theory, which describes the composite as having global planes of weakness or "action planes" (see Lutz, 2006, for a description).

Analysis of the distribution of stresses that result from the action of an applied external load within the matrix material surrounding an embedded inhomogeneity, such as a fiber, reveals regions of stress magnification or concentration. The repeating periodic arrangement of a fiber embedded in a matrix serves to collectively activate these regions of stress magnification or "action planes." Figure 3 shows an example of the pattern of stress magnification that is predicted to occur for a periodic arrangement of fibers within a matrix. The figure shows FEA results from a 3-by-3 square-packed array of fibers embedded in a matrix for a PMC loaded under transverse tensile stress (applied top to bottom). A CMC would exhibit different, but analogous, patterns of stress magnification because of the relative dissimilarity in the mechanical properties of the constituent materials. Localized regions of open porosity (that can be many times larger than the RUC itself) will act collectively, or equivalently, as a larger sized flaw and serve to initiate failure about an action plane when the applied stress acting on that plane reaches a critical level. Regardless, in this report we assume that the Weibull distribution is a good approximation for the strength distribution of the individual material constituents and that stress concentrations that are predicted to exist within the RUC are real and affect the overall failure response of the composite under multiaxial loading.
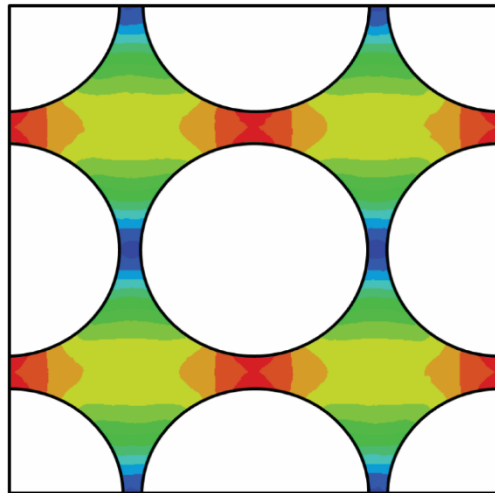

Figure 3.—Finite element analysis results for a 3-by-3 square-packed array of fibers embedded in a matrix for a polymer matrix composite (PMC) loaded under transverse tensile stress (applied top-to-bottom) showing a pattern of stress magnification. From the results of Nemeth (2013a, 2014b).

3.1 FEAMAC/CARES Program Architecture and Stochastic Damage Methodology

FEAMAC/CARES combines the MAC/GMC micromechanics analysis and the CARES/*Life* brittle material life prediction capabilities into the FEAMAC framework of an Abaqus UMAT. Because CARES/*Life* is run within MAC/GMC as a callable user subroutine, only minor modifications to the original FEAMAC code were required. However, extensive use was made of common block storage arrays to hold information relevant to CARES/*Life* that is associated with the finite element model. FEAMAC, MAC/GMC, and CARES/*Life* are written in the Fortran computer language, and to date, FEAMAC/CARES has only been executed on the Microsoft Windows 7 (64-bit) platform. FEAMAC/CARES requires both CARES/*Life* and MAC/GMC input files to provide information on the constituent materials (e.g., elastic properties, failure criteria parameters, statistical parameters, and RUC geometry). Multiple CARES/*Life* failure modes may be selected for a given material.

FEAMAC/CARES has a substantial memory storage requirement. This was implemented to avoid the slow process of searching, reading, and writing information to files. However, the penalty is a memory requirement that must be scaled with the size of the finite element model and the number of time steps. The storage arrays become large quickly because of the need to systematically bookkeep all the information necessary to execute the problem. For example, stresses and temperature are stored for every subcell of the RUC for every element integration point for all elements and time steps. CARES/*Life* needs all of this information every time that it is run for a specific subcell and specific time step. It needs to know the previous stress history and time increments to predict the life of the subcell at the current time step. Heap arrays are used for the largest arrays. Array sizes can be easily adjusted to fit the need, but the Fortran source code must be recompiled every time that such an adjustment is made.

Figure 4 shows a schematic of the interoperation of CARES/*Life* with MAC/GMC and Abaqus. Element integration points are processed before the simulation proceeds to the next element, and all elements are processed sequentially before the simulation proceeds to the next time step. Figure 4 also indicates how the damage response develops and accumulates in FEAMAC/CARES as the simulation proceeds through the time steps. Figure 5 also helps to explain this process. Damage is implemented by reducing the elastic stiffness constants for a given subcell. Here we assume that either the subcell is completely intact or that it has completely failed. If it has failed, then the elastic constants are reduced to an arbitrarily chosen low value. In the present work this is assumed to be 1 percent of the original undamaged values. In MAC/GMC this is handled by a damage parameter that is allowed to range between 1.0 (undamaged) and 0.0 (complete failure). In FEAMAC/CARES, when the subcell failure condition is reached, this parameter value is changed from 1.0 (the undamaged state) to 0.01 (a mostly damaged state) as a step function. (The value of 0.01 is used instead of 0.0 to avoid numerical problems with the solution process.) This version of FEAMAC/CARES uniformly reduces the Young's and shear moduli in all directions. Anisotropic stiffness reduction, where the direction of applied loads affects the orientation of resultant damage, is not considered.

The determination of whether to fail subcells at a given time step is made at the material level of the RUC: that is, the total probability of failure of all subcells in the RUC for a given material (at a particular element integration point) is computed and then compared with a random number between 0 and 1. The random number is generated according to a uniform distribution. This is equivalent to assigning a random failure probability (or a random probability for a damage initiation event to occur) for that material at that element integration point. A set of uniformly distributed random numbers varying between 0 and 1 is generated for each material in the RUC for each element integration point during the initialization of FEAMAC/CARES. Once set, these values remain unchanged for the entire simulation execution. We henceforth refer to a single member of this set for a particular material j as $P_{f,j(\text{random})}$. In Figure 5, when the failure probability $P_{f,j(\text{CARES})}$ of material j of the RUC calculated using CARES/*Life* for the element integration point is equal to or exceeds the a priori assigned failure probability $P_{f,j(\text{random})}$ of material j of the RUC for the element integration point, then all the subcells of material j in that RUC are considered to have failed and their elastic modulus is reduced by 99 percent for subsequent iterations.
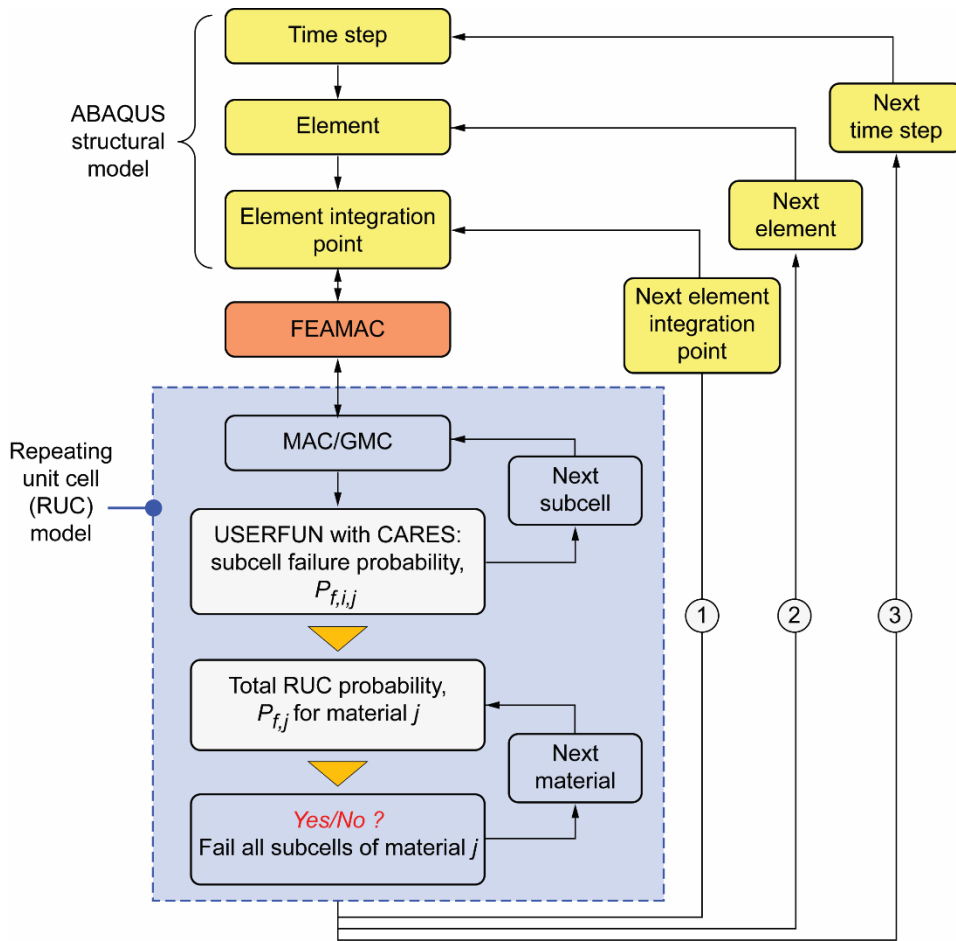
Figure 4.—Interoperation of CARES/*Life* with MAC/GMC and Abaqus. Element integration points are processed first (loop 1) before the simulation proceeds to the next element (loop 2), and all elements are processed sequentially before the simulation proceeds to the next time step (loop 3).
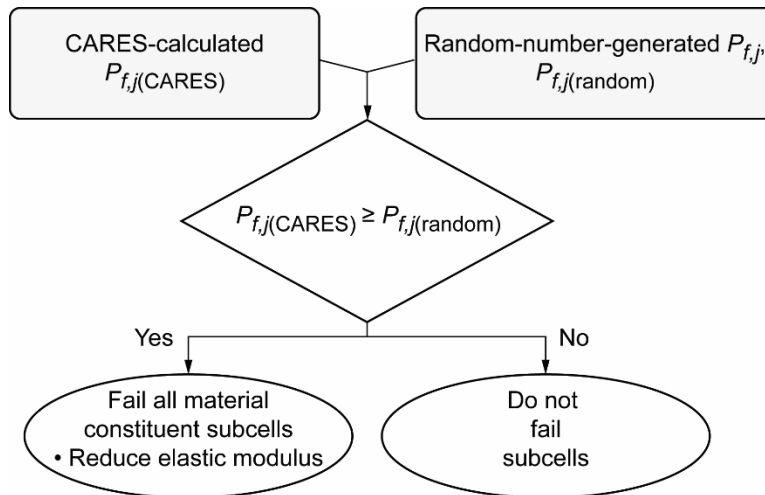

Figure 5.—Material constituent *j* failure evaluation in the repeating unit cell (RUC) for a given element integration point and time step comparing the CARES-calculated probability of failure $P_{f,j(CARES)}$ with a random-number-generated $P_{f,j(random)}$ associated with the material failure response at that integration point.

It is much easier to use a random number generator to associate a material with a probability of failure or probability of damage initiation event than to use a random-number-generated strength (from an underlying probability distribution of material strength) such as was done in Iarve et al. (2011). This is because an approach using a random probability of failure avoids the issues of random flaw orientation, the presence of stress gradients or changing stress states over the material domain of interest over time, and changing direction of applied load over time. For a given material subcell, randomly generated strengths that seed the material with intrinsic flaws must also account for the probabilistic-based orientation of the flaw. This is an unnecessary complication. We avoid this problem by simply associating a random failure probability with the material element, which is independent from issues such as the orientation of the flaw relative to the direction of the applied loading.

The meaning of the inequality in Figure 5 follows: The $P_{f,j(\text{random})}$ associated with the material failure response of material j at that integration point is analogous to the probability that a flaw of critical strength σ_c *or less* exists (in a uniform stress field of equivalent or effective volume V_e (see Nemeth et al., 2003, 2005)) and that it is oriented relative to the loading such that it would initiate damage propagation and locally fail the material. CARES/*Life* is used to calculate this probability, based on its probabilistic failure criteria, for a given level and distribution of applied stresses over the RUC material. The previously generated $P_{f,j(\text{random})}$ (generated as an initial condition before the load sequence was applied) corresponds to a flaw that is assumed to exist of critical strength σ_{cr} oriented relative to the loading field. This "seeds" the material with an equivalent strength of flaw. That flaw strength, σ_{cr} *or less*, has a probability of existence $P_{f,j(\text{random})}$ associated with it. If the equivalent threshold stress σ_{1eq} from the applied loading, equal to the strength σ_c (as implied from CARES/*Life*), exceeds or is equal to the assumed-to-be-present flaw of strength σ_{cr}, then that flaw will propagate and fail the material locally in the RUC.

The reasons why we evaluate failure at the material level of the RUC rather than at the individual subcell level has to do with the process of failure. MAC/GMC does not explicitly model crack growth, instead it uses the reduction in stiffness that is associated with damage. In reality, when dealing with brittle material, local failure tends to be abrupt and complete (i.e., a crack path through the RUC material constituent at a given FEA element integration point). Progressive failing by individual subcells in the RUC means that the failure process can be sensitive to the number and arrangement of the subcells. A more detailed RUC model with more subcells could have a different response than a less detailed RUC. Evaluating failure at the material level, rather than at the local subcell level, reduces the sensitivity to the subcell density in the RUC. However, this model will still be sensitive to how well the peak stresses near the stress concentrations are reproduced. This means that stress field accuracy or granularity with subcell density will affect results. Failing (or abruptly reducing the stiffness of) the whole material constituent in the RUC better approximates local catastrophic failure. Damage over the whole structure may develop gradually, depending on the composite architecture and loading, but damage locally is more likely to be total (at least in terms of a complete loss of stiffness) for the particular material constituent (fiber failure or matrix failure) at a particular element integration point.

For example, in a tensile specimen consisting of 0° unidirectional plies under uniaxial tension, overall damage (the change in the stress-strain response) to the specimen develops gradually from distributed microcracking in the matrix. However, at the local level of the RUC where a microcracking event takes place, the effect is more dramatic and sudden—affecting the material in a more brittle-like manner. So, locally damage would be sudden, abrupt, and brittle-like, whereas at the global level of the structure, total damage would accumulate more slowly from all the discrete microcracking events. This is shown schematically and analytically in Ahn and Curtin (1997).

The FEAMAC/CARES methodology relies on subcell-level stress fields (rather than mean constituent fields) to determine the probability of constituent failure. To determine the failure probability of a material in the RUC, one must consider the combined effect of all of the material subcells together. This is explained as follows: CARES/*Life* is called from MAC/GMC to calculate a probability of failure $P_{f,i,j}$ (or conversely the probability of survival $P_{s,i,j}$ or reliability, where $P_{s,i,j} = 1 - P_{f,i,j}$) for a given subcell i

(composed of material *j*) of the RUC for the respective element integration point and the particular time step. The probability of survival $P_{s,j}$ for material *j* of the RUC is the product of the probability of survival of all the subcells of material *j*:

$$P_{s,j} = \prod_{i=1}^{n} P_{s,i\,j} \tag{1}$$

where *n* is the total number of subcells of material *j* in the RUC. Note that, to avoid numerical problems, Equation (1) is actually evaluated using the risk-of-rupture (ROR) summation as described in Nemeth et al. (2003, 2005). ROR is discussed in Section 3.2 of this report (see Eq. (2)). Equation (1), which is shown because of its simplicity, is a "weakest link" assumption whereby the weakest link that will cause the whole analogous chain to fail is recalculated at each time step. Because of the transient analysis capability of CARES/*Life* as described in Nemeth et al. (2005), failure probability will never decrease at a subsequent load step regardless of the magnitude of the applied loading: that is, the calculations are history dependent (when the proper input parameter settings are used). When the failure condition indicated in Figure 5 is met, then all subcells in the material for the RUC are failed and the failure probability for the material becomes 1.0 (failed). This condition is maintained for subsequent time steps and no further CARES/*Life* evaluations are performed for that material of the RUC for that element integration point.

When we use Equation (1) to evaluate the potential for local material failure of the RUC, we avoid the issue of a stochastic toughening mechanism (e.g. Planas, 1995; Bazant and Planas, 1998) at the subcell level. However, this issue still remains at the element integration point level—where it is likely that integration points adjacent to a failed point have a $P_{f,j\text{(random)}}$ (per material *j*) that is higher than that of the failed point. We say "likely" because that statement also depends on factors such as the presence of local stress gradients, the size of one element compared with another (the size effect issue), the changing multiaxial stress field, and the presence of possible temperature gradients where material properties or parameters may change with temperature. In order to be able to control the stochastic toughening mechanism at the element integration point and element level another feature was added to FEAMAC/ CARES so that the elements directly adjacent to an element that contains at least one failed integration point could be identified and that some of their respective element integration point random-number-seed failure probabilities could be made equal to (or alternately to approach) that of element integration points (for that material) where failure occurred (according to the failure criterion shown in Fig. 5). This adjacent-element-failure feature encourages a more abrupt physical failure and the development of a more cracklike damage growth pattern. We call this type of procedure the cellular-automaton adjusted-element technique. A cellular automaton is a collection of designated cells on a grid that evolve through discrete time steps according to a set of rules based on the states of neighboring cells.

Figure 6 shows an example comparison of damage accumulation with and without this user-adjustable feature for a 25×25 finite element mesh of S4R shell elements representing a single 0° ply loaded in uniaxial tension (with the loading and fiber direction indicated by arrows).

Figure 6(a) shows a color sequence of how elements adjacent to a failed element are categorized. In the center of the figure is an element that has at least one failed matrix element integration point. The elements directly adjacent to the element with a failure are also shown. These elements share at least one common node with the element with a failure. A simple search routine was used to read a file (a user-prepared text file) containing all of the element nodal connectivities and to identify the elements that share at least one common node with the element containing a matrix failure.

The procedure for adjusting adjacent-element integration-point probability of failures follows: At the beginning of a time step *i* + 1, the values of $P_{f,j}$ for all elements for all materials are calculated from the subcell values of $P_{f,i,j}$ for the previous time step *i*. If, for some element integration point the failure condition is fulfilled, then that integration point material is flagged as having failed (within the MAC/GMC program). In this case, the value of $P_{f,j}$ is set to 1.0 for the current and subsequent time steps, and no
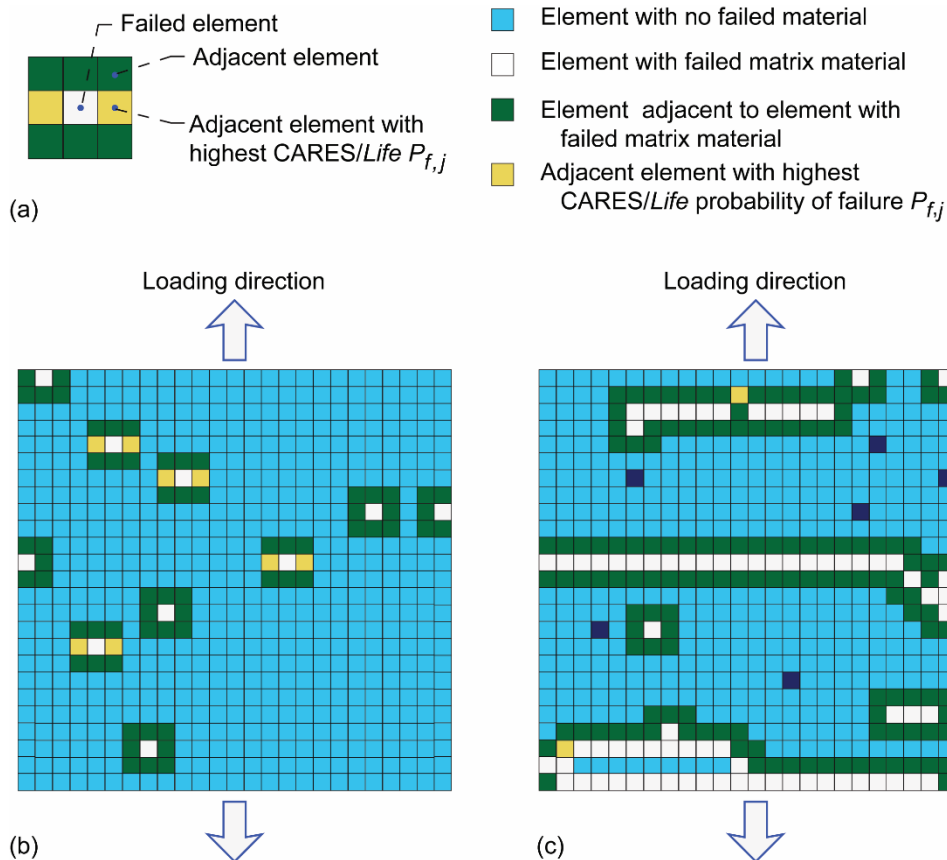
Figure 6.—Example of the adjacent-element-failure feature for a matrix failure of a 0° composite loaded in tension, showing adjacent elements with the highest probability of failure $P_{f,j}$. (a) Elements adjacent to a failed element. (b) Random element failure—no adjustment of adjacent element failure probabilities. (c) Random element failure with adjustment of adjacent element failure probabilities.

further CARES/*Life* failure probability calculations are performed for that element integration point. The $P_{f,j(\text{random})}$ of the other integration points in that element are made equal to that of the failed element integration point (for that material). This eliminates local within-element toughening effects.

The integration points of elements that are adjacent to the element that contains a failed integration point are flagged. FEAMAC/CARES then proceeds through all the elements for the $i + 1$ time step. At the beginning of the $i + 2$ time step, all $P_{f,j}$ for all integration points for all elements are again calculated according to Equation (1), except for previously failed integration points. Reducing the stiffness of failed materials set at time step i will cause stresses to redistribute locally around failed element integration points at the subsequent time step $i + 1$. This stress redistribution affects the probability of failure $P_{f,j}$ of the integration points of the adjacent elements, which are calculated at the beginning of time step $i + 2$. At this point, the maximum value of each integration point $P_{f,j}$ is determined for each element that is adjacent to a previously failed element. The two elements with the maximum $P_{f,j}$ from the set of adjacent elements are flagged, and their respective element-integration-point $P_{f,j(\text{random})}$ for that particular material are made equal to the $P_{f,j(\text{random})}$ associated with the previously failed element integration point. This is indicated in Figure 6(a). If one adjusts only the random-generated failure probabilities for two adjacent elements, a more physical, cracklike (planar) growth pattern can emerge as FEAMAC/CARES proceeds through subsequent time steps.

Figures 6(b) and (c) show examples of how this damage process progresses after several time steps for an applied uniaxial displacement load for a 0° unidirectional ply for a CMC (based on the properties described by Goldberg, 2012, and Weibull statistical strength parameters consistent with ceramic materials). Figures 6(b) and (c) show instances of matrix failure. Figure 6(b) shows random failures with the adjusted element failure probability feature turned off. Adjacent elements are still indicated according to the rules outlined for Figure 6(a). It is clear that damage is distributed or diffused and is not propagating rapidly (failure instances are isolated). Figure 6(c) shows damage progression through several time steps with the feature fully turned on. Here damage is more organized, and a more linear (less diffused) and cracklike growth pattern emerges. This pattern is more representative of the physical failure process and has proven to provide better failure predictions for brittle materials. As will be shown, the cellular-automaton adjusted-element procedure also affects how quickly the stress-strain response changes with subsequent time steps.

3.2   CARES/*Life* Methodology Overview

A brief overview of the CARES/*Life* methodology is provided to explain the conceptual basis of the approach. A full description, including all the parameters necessary for the calculation of probability of failure is found in various references. Nemeth et al. (2005) describes the Batdorf unit sphere methodology for brittle materials with isotropic failure strength and extends the methodology for fully transient (loads changing over time) situations. Nemeth (2013a, 2014a) introduces mechanisms of flaw orientation anisotropy and fracture toughness orientation anisotropy to account for brittle materials with transversely isotropic failure strength, and Nemeth (2013b, 2014b) applies this methodology to an RUC of a fiber-in-matrix PMC to show how the stress interactions within the RUC influence the overall multiaxial failure response of the composite. The Appendix describes the symbols used here.

The Batdorf methodology (see Nemeth et al., 2005 for a more complete description) in CARES/*Life* uses the Weibull distribution (Weibull, 1939a, 1939b) to describe the brittle material stochastic failure response. This includes how failure probability is affected by the volume of material that is under loading—the so-called size-effect. The Batdorf theory offers a physical mechanism to account for the effect that multiaxial stresses have on the stochastic failure response of an isotropic brittle material.

The two-parameter Weibull equation describes the probability of failure of a part under loading as

$$P_{fV} = 1 - \exp\left[\int_V \left(\frac{\sigma(x, y, z)}{\sigma_{oV}} \right)^{m_V} dV \right] = 1 - \exp\left[-ROR \right] \tag{2}$$

where x,y,z is the point location in the structure under applied stress σ at that point, V is the volume, σ_{oV} is the scale parameter, and ROR denotes the risk of rupture. The subscript V denotes a quantity that is a function of volume. With the two-parameter model, the scale parameter σ_{oV} corresponds to the stress level where 63.21 percent of tensile specimens with unit volumes would fracture. The scale parameter σ_{oV} has dimensions of stress $\times$ (volume)$^{1/m_V}$, and m_V is the shape parameter (Weibull modulus)—a dimensionless parameter that measures the degree of strength variability. As m_V increases, the dispersion is reduced. These three statistical parameters are considered to be material properties, and they are temperature and processing dependent. The Weibull parameters in Equation (2) represent inert (fast-fracture) strength parameters. The effect of time- or cycle-dependent SCG requires additional modeling, as has been done in Nemeth et al. (2003, 2005), for example. Equation (2) defines the Weibull stress-volume integral.

In FEAMAC/CARES the summation of the individual subcell *ROR* values gives the overall *ROR* for the material in the RUC, as was previously mentioned with regard to Equation (1). This summation of subcell *ROR* avoids the numerical problems associated with the multiplication operations in Equation (1) when subcell reliabilities are very close to 1.0 in value, which causes the loss of significant digits in single precision and double precision multiplication calculations where reliabilities are 0.9999 and higher.

Another important item to consider is that Equation (2) requires knowing the volume of material under stress. In FEAMAC/CARES, element volume is not directly accessible. Instead a "characteristic element length" (CELENT, an argument passed from Abaqus), which is equal to the cube root of the element volume for a solid element or the square root of the surface area of a shell element, is used. The volume associated with the element integration point is approximated as the element volume (as calculated from CELENT and the element type) divided by the number of integration points in the element. This does not account for distortions in an element's geometry. However, it is most likely a conservative assumption because integration point volumes in highly distorted elements with stress gradients (around stress concentration features) usually have smaller volumes associated with the highest stressed points (the points closest to the stress concentration feature) in comparison to the other integration points in the element. A further complication is that the MAC/GMC subcells also have their own volume or area associated with them that is independent of Abaqus (dependent on the construction of the RUC in the MAC/GMC input deck). In FEAMAC/CARES the subcell volume is automatically adjusted to be equal to the ratio of the subcell volume to the total RUC volume.

3.2.1 Batdorf Unit Sphere Multiaxial Stochastic-Strength Theory for Isotropic Materials

The Weibull equation assumes that catastrophic crack propagation initiates from a critically loaded flaw; however, it does not describe the physical mechanism behind this phenomenon. Batdorf and Crose (1974) and Batdorf and Heinisch (1978) addressed this shortcoming by combining the weakest-link theory (WLT) with linear elastic fracture mechanics (LEFM). Batdorf developed his theory to account for the effect of multiaxial stress states on brittle materials. He provided an improved physical basis for failure by incorporating an assumed crack geometry, mixed-mode fracture criterion, and a crack orientation function. In addition to the previously cited Batdorf references, a full treatment of the Batdorf theory can be found in Nemeth et al. (2003, 2005). The Batdorf theory has been developed for volume-residing flaws (failure probability as a function of material volume) as well as for surface-residing flaws (failure probability as a function of material surface area), again detailed in Nemeth et al. (2003, 2005). FEAMAC/CARES does not consider surface-residing flaws.

In the Batdorf unit-sphere theory, flaws are assumed to be randomly oriented. Under the action of an applied multiaxial stress state, the probability that a flaw will be oriented such that it will initiate crack growth can be calculated. This involves an equation for an effective, or equivalent, stress σ_{Ieq}, which is a function of an assumed preexisting flaw shape (like a penny-shaped crack) and mixed-mode fracture criterion. The effective stress is the equivalent amount of stress on the flaw loaded in Mode I (crack-opening mode) that will initiate Mode I crack growth. A direction normal to the flaw plane can be defined with angular coordinates α and β defined in a global coordinate system reference frame, as shown in Figure 7. We represent that direction as an (infinitesimally small) incremental area element dA projected on a sphere with a radius of length 1.0 (a unit sphere). We can then determine the probability that the flaw will be oriented such that crack growth will be initiated from the applied far-field multiaxial stress state Σ by integrating over the entire surface area of a unit-radius sphere, representing all possible orientations of the flaw (Fig. 7).

In other words if we project onto the spherical surface the equivalent (effective) stress $\sigma_{Ieq}(\Sigma, \alpha, \beta)$, then the fraction of the total area of the unit sphere containing all the projected equivalent stresses satisfying $\sigma_{Ieq} \geq \sigma_{Ieqc}$ represents the probability that a flaw of strength σ_{Ieqc} will cause crack growth to be initiated, where σ_{Ieqc} denotes an effective (or equivalent) critical mode I stress from the applied multiaxial stress state.
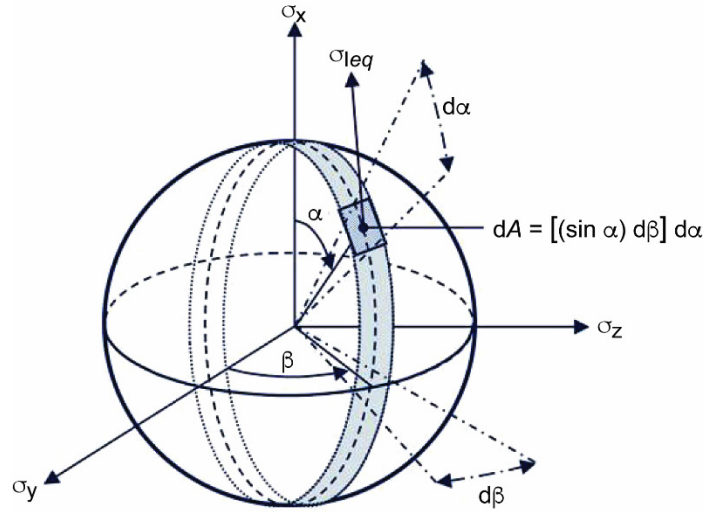
Figure 7.—Projection of equivalent stress onto a unit radius sphere in the global coordinate system stress space. The unit radius sphere represents all possible flaw orientations, where σ_{Ieq} is an effective stress, and α and β are angular coordinates. An infinitesimal area dA on the unit sphere represents a particular flaw orientation (a direction normal to the flaw plane), and σ_{Ieq}, the equivalent stress, is a function of an assumed crack shape and multiaxial fracture criterion.

The effective stress σ_{Ieq} represents an equivalent normal stress on the crack face from the combined action of the normal stress σ_n and the shear stress τ on the microcrack oriented at the angular coordinates, α and β (see Fig. 7). For the sake of brevity, the development of the effective stress equations is not shown here (for details, see Nemeth et al., 2003, 2005). In an isotropic material for a penny-shaped crack with the Shetty mixed-mode fracture criterion (Shetty, 1987), the effective stress becomes

$$\sigma_{Ieq} = \frac{1}{2}\left\{ \sigma_n + \sqrt{\sigma_n^2 + \left[\frac{4\tau}{\overline{C}(2-\nu)}\right]^2} \right\} \tag{3}$$

where ν is Poisson's ratio and $\overline{C}$ is the Shetty shear-sensitivity coefficient, with values typically in the range $0.80 \leq \overline{C} \leq 2.0$. As $\overline{C}$ increases, the response becomes progressively more shear insensitive. Shear increases the equivalent stress as shown in Equation (3), and this has a deleterious effect on the predicted material strength. The value of $\overline{C}$ can be fit empirically to experimental data—either on introduced cracks (as was done in Shetty (1987)) or on specimens being tested multiaxially. Equation (3) is for a tensile mode of failure (when σ_n is tensile) on the unit sphere. For a compressive mode of failure (when σ_n is compressive) on the unit sphere, a simple Tresca-like criterion can be used:

$$\sigma_{Ieq} = 2\tau \tag{4}$$

which would be modeled as a separate failure mode with its own parameter description set, where τ is the shear stress acting on a crack plane.

Integrating σ_{Ieq} over the surface area of the unit sphere, and V results in Equation (5) (see Batdorf, 1978; Batdorf and Heinisch,1978; Nemeth et al., 2003, 2005):

$$P_{fV} = 1 - \exp\left[-\frac{\bar{k}_{BV}}{2\pi} \int_V \int_0^{2\pi} \int_0^{\pi/2} \left(\frac{\sigma_{Ieq}(x,y,z,\alpha,\beta)}{\sigma_{oV}} \right)^{m_V} \sin\alpha \, d\alpha \, d\beta \, dV \right] \tag{5}$$

where m_V is the shape parameter, σ_{oV} is the scale parameter, and $\bar{k}_{BV}$ is the normalized Batdorf crack-density coefficient (which makes Eq. (5) equal to Eq. (2) for a uniaxial stress state). In CARES/*Life* the normalized Batdorf crack density coefficient $\bar{k}_{BV}$ is an internally calculated value and is not supplied by the user. For a given incremental volume, $\sigma_{Ieq}(x, y, z, \alpha, \beta)$ is the projected equivalent stress over the unit radius sphere in stress space as depicted in Figure 7 for location coordinates x, y, and z within the body. Equation (5) is a form of the Weibull distribution that was modified to account for the effect of multiaxial stresses. In FEAMAC/CARES this equation is evaluated to determine the $ROR_{i,j}$ for $P_{f,i,j}$ at the subcell level of the RUC at the element integration point. The summation of all $ROR_{i,j}$ for material j of the RUC gives the ROR_j of the material. Equation (5) is the Batdorf "unit sphere" equation for isotropic failure strength material constituents.

3.2.2   Analysis With Time Steps and Time-Dependent Strength Degradation

FEAMAC/CARES analyzes material integrity at a given instance of time. It performs these calculations at successive time increments (time steps). Damage that is initiated at a previous time step is maintained at a successive time step and allowed to propagate or accumulate at that step. In this manner, damage can accumulate and propagate as the analysis advances through the time steps. The failure probability calculation of the unit sphere method shown in Equation (5) is only applicable for loading at any instant of time and does not consider previous loading history. This is acceptable in FEAMAC/CARES for the fast-fracture failure mode but not for a time-dependent (or cycle-dependent) failure mode, where prior loading history must be considered to assess the potential for failure at some instance in time. CARES/*Life* has methodology to predict the probability of failure over successive time steps for time- and cycle-dependent loading that can be used for fatigue life prediction or life prediction at a constant load. This is described in Nemeth et al. (2005). The following is a brief summary.

SCG refers to the stable extension of a crack over time. Similar to stress corrosion in metals, SCG is a result of the combination of stress at the crack tip and chemical attack or loosening of viscous phases (at high temperature) such that chemical bonds at the crack tip break or material displaces and the crack tip extends. The crack length a as a function of time t can be expressed as a power law of the equivalent mode I stress intensity factor K_{Ieq} (from applied stress state Σ) with the following form

$$\frac{da}{dt} = A \, K_{Ieq}^N \tag{6}$$

where A and N are material parameters that depend on the temperature and environment. In a transient loading analysis, the temperature and/or environment can vary with time and location causing A and N to change accordingly.

Equation (6) can be modified to include a cyclic fatigue degradation component as was done in Rahman et al. (1998) (and reproduced in Nemeth et al., 2005) so that

$$\frac{da}{dt} = \left[A_1 \, g + f_c A_2 (1-R)^Q \right] K_{Ieq,\max}^N \tag{7}$$

where $A_1 = A$ in Equation (6), A_2 is a constant, f_c is the cyclic loading frequency, R is the R-ratio of minimum to maximum stress in a cycle, Q is the Walker fatigue law R-ratio sensitivity exponent, g is a constant related to the shape of the cyclic loading waveform (see Nemeth et al., 2003, 2005, for example), and $K_{Ieq,\max}$ is the maximum value of K_{Ieq} in the loading waveform. Equation (7) is limited to steady-state cyclic loading.

In many engineering applications, structural components are subjected to repeated block loading. A load block indicates a collection of several load cycles. Such repeated cyclic loading and its effect on damaging the ceramic structural component can be incorporated into the transient reliability analysis. Nemeth et al. (2005) have developed a much more computationally efficient means to perform this task for power law SCG. This approximation method allows for a tradeoff between solution accuracy and numerical efficiency. The methodology allows a load block to consist of an arbitrary number of cycles, and a solution can be obtained using only one load block or as many load blocks as desired.

For a given material, the Weibull constants, m_V and σ_{oV}, and the SCG parameters, N_V and B_V, are the necessary input parameters for the CARES/*Life* transient analysis for the power-law formulation of SCG of Equation (6). The parameter N_V is the volume-flaw crack-growth constant exponent, and B_V is a fatigue constant derived from constant A in Equation (6) (see Nemeth et al., 2005).

$$B_{V,k} = \frac{2}{A_k \, Y^2 \, K_{Ieqc,k}^{N_{V,k}-2} \left(N_{V,k} - 2\right)} \tag{8}$$

Here Y is the crack geometry correction factor or shape factor, and $K_{Ieqc,k}$ is the critical equivalent mode I stress-intensity factor from the applied multiaxial stress at time step k. The Weibull constants, m_V and σ_{oV}, and the SCG parameters, N_V and B_V, are input into CARES/*Life* as a function of temperature. The parameter values are linearly interpolated from the input values for element integration point temperatures during an analysis. For fast-fracture reliability analysis, only the Weibull constants, m_V and σ_{oV}, are required.

There are some issues or inconsistencies when applying the SCG model to FEAMAC/CARES. One is that a crack can grow under SCG to a comparatively large size relative to the RUC, and even relative to the involved finite element, prior to reaching a critical size where mechanical resistance to crack growth at the crack tip is exceeded (particularly at high temperatures in ceramics). This situation is not accounted for in FEAMAC/CARES. The effect of stress gradients that can occur along the crack length also is not considered, and SCG strength degradation can occur at different rates in adjacent elements in the presence of temperature gradients and/or stress gradients. Finally, the SCG model in CARES/*Life* does not consider the effect of fiber bridging traction on matrix SCG. This is only indirectly considered in FEAMAC/CARES from elastic modulus stiffness degradation—where the homogenized (including the cumulative effect of all material constituents in the RUC) elastic modulus of the element integration point would degrade less if material phases like the fiber(s) remained intact. Less stiffness degradation also means that less stress concentration will result in surrounding elements, and that reduces the tendency of those elements to fail (depending on circumstances like the presence of stress gradients or if the "adjusted element" feature is active or not).

3.2.3 Batdorf Unit Sphere for Anisotropic Failure Strength

The individual brittle material constituents of the RUC can be considered as separate monolithic material phases; however, that does not mean that they are isotropic in strength. Having the ability to account for anisotropic strength provides the flexibility necessary to be able to adjust a model to available experimental data. The CARES/*Life* algorithm has been modified to predict the failure response for anisotropic material constituents. This includes the Tsai-Hill and Tsai-Wu multiaxial failure criteria expressed in terms of a Weibull distribution (with transient analysis capability) as well as the Batdorf unit

sphere methodology. Nemeth (2013a,b; 2014a,b) extends the Batdorf unit sphere methodology for materials having anisotropic strength. This study investigated the capability of the unit sphere methodology to predict the failure response of a finite element model of an RUC for a unidirectional PMC under biaxial loading.

Two different physical mechanisms were considered in order to extend the unit-sphere model to account for anisotropic strength: (1) flaw-orientation anisotropy, whereby a preexisting microcrack has a higher likelihood of being oriented in one direction over another, and (2) critical strength or fracture toughness anisotropy, whereby the level of critical strength σ_{Ic} or fracture toughness K_{Ic} for mode I crack propagation changes with regard to the orientation of the microstructure. The equations developed to characterize these properties are general and can model tightly defined or more diffused material anisotropy textures describing flaw populations.

Flaw-orientation anisotropy refers to the situation where a flaw has a higher likelihood of being oriented in one direction than another for a given critical strength. Thus, a material will be stronger on average in one direction than another. An isotropic brittle material is equally strong in any direction, and thus its flaws are uniformly randomly oriented. However, for components made by processes such as extrusion or hot-pressing, which induce texture, a bias will exist in the orientation distribution of the processing flaws. Also, components finished by surface grinding will contain machining damage in the form of surface cracks that are oriented parallel and transverse to the grinding direction. For composite materials, the interface, or an interfacial layer between the fiber and the matrix, can act as a flaw with an orientation bias that induces an anisotropic failure response.

For volume-distributed flaws, flaw-orientation anisotropy relative to a material coordinate system is modeled by introducing a probability density function (PDF) into the unit-sphere formulation. In Figure 8, we represent two different flaw populations by a "polar-cap," or longitudinal L distribution of flaws and by an "equatorial-belt," or transverse T, distribution of flaws. The polar-cap distribution describes crack planes symmetrically distributed (centered) about a plane (in this case the σ_y–σ_z plane), and the equatorial-belt distribution describes crack planes symmetrically distributed (centered) along a line (in this case, the σ_x axis). Further details with equations are provided in Nemeth (2013a,b). Figure 8 shows the unit sphere with separate PDFs describing the anisotropy of the flaw orientation, where α and β are angular coordinates and Λ_L and Λ_T are constants in the flaw-orientation anisotropy function representing longitudinal and transverse distributions. Orientation is described with the normal to the crack plane.

The separate polar-cap and equatorial-belt distributions are introduced to describe individual, and distinctly different, failure modes. For a unidirectional fiber-reinforced composite, the polar cap can be used to represent the fiber strength distribution. For a laminate it can represent the interfacial flaws between the layers (flaws aligned parallel to the interface associated with delamination). The equatorial belt can be used to represent the matrix-fiber interface. The equatorial-belt and the polar-cap distributions can be considered to equivalently represent global failure planes, which are referred to as "action planes" in the Puck multiaxial strength model for composites.

In the critical strength or fracture toughness anisotropy model, the critical stress intensity factor (mode I fracture toughness) K_{Ic} varies with the orientation angle on the unit sphere. This is functionally equivalent to σ_{Ic} varying with orientation, and it is also functionally equivalent to the size of the flaw changing with the orientation angle. For a CMC, where damage from tensile loading manifests itself as a periodically spaced matrix cracking with fiber bridging, fracture toughness cannot be defined on the global scale of the structure. However, it is acceptable to use fracture toughness on the local scale at the matrix crack tip, where micromechanics can account for the bridging explicitly. In this report, the mechanisms involved with fiber bridging are not considered. Of significance herein is that the local fracture toughness could be allowed to vary with the orientation of the flaw plane (or action plane) and the applied loading.
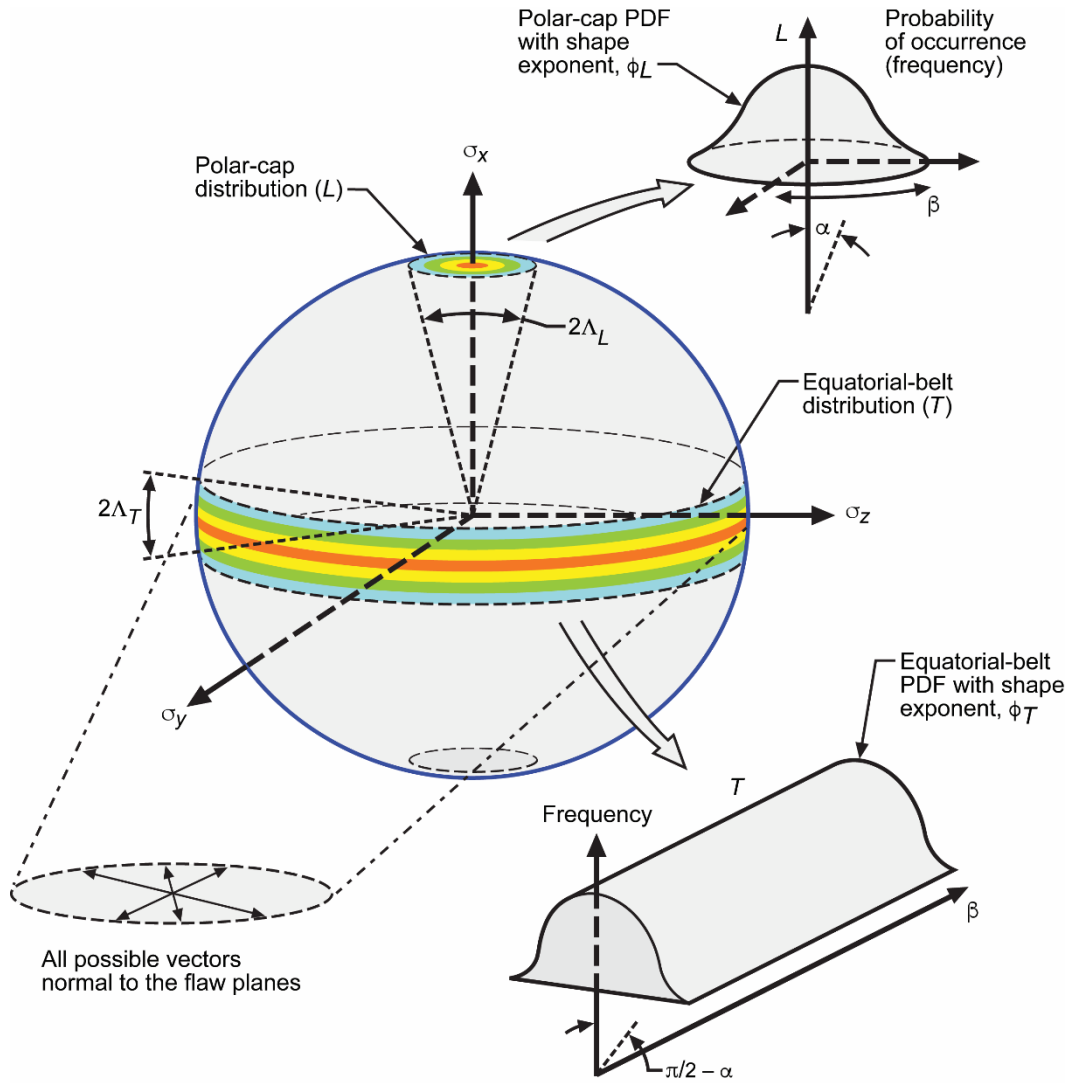
Figure 8.—Unit sphere with probability density distribution functions (PDFs) describing the anisotropy of the flaw orientation, where α and β are angular coordinates and Λ_L and Λ_T are constants in the flaw-orientation anisotropy function representing longitudinal (polar cap) and transverse (equatorial belt) distributions. (See Nemeth 2013a, 2013b, 2014a, 2014b for details.)

The fracture-toughness-anisotropy equations for a transversely isotropic strength response are constructed following a convention similar to that in Figure 8, with separate polar-cap and equatorial-belt formulations. This is shown in schematically in Figure 9. A function, $\bar{f}_{\mathrm{I}c}(\alpha)$ is defined that normalizes critical mode I loading strength $\sigma_{\mathrm{I}c}$ as a function of flaw orientation angle α. The critical strength $\sigma_{\mathrm{I}c}$ is proportional to fracture toughness $K_{\mathrm{I}c}$, and $\sigma_{\mathrm{I}c,\max}$ is the maximum value of $\sigma_{\mathrm{I}c}$ over the unit sphere (for all α). The term $\bar{f}_{\mathrm{I}c}(\alpha)$ is a normalized function expressing the degree of this anisotropy with the orientation of the flaw. The L subscript relates to the polar-cap strength anisotropy distribution for crack planes symmetrically distributed (centered) about a plane (in this case, the σ_{y}–σ_{z} plane), and the T subscript relates to the equatorial-belt strength anisotropy distribution for crack planes symmetrically distributed (centered) along a line (in this case the σ_{x} axis). Here, ξ_L, ξ_T, γ_L, and γ_T are constants in the critical mode I stress intensity anisotropy function representing longitudinal and transverse distributions; and $\overline{\sigma}_{\mathrm{I}c,\mathrm{x}}$, $\overline{\sigma}_{\mathrm{I}c,\mathrm{y}}$, and $\overline{\sigma}_{\mathrm{I}c,\mathrm{z}}$ are the normalized (by $\sigma_{\mathrm{I}c,\max}$) orthogonal critical strength components. Further details with equations are provided in Nemeth (2013a,b, 2014a,b).
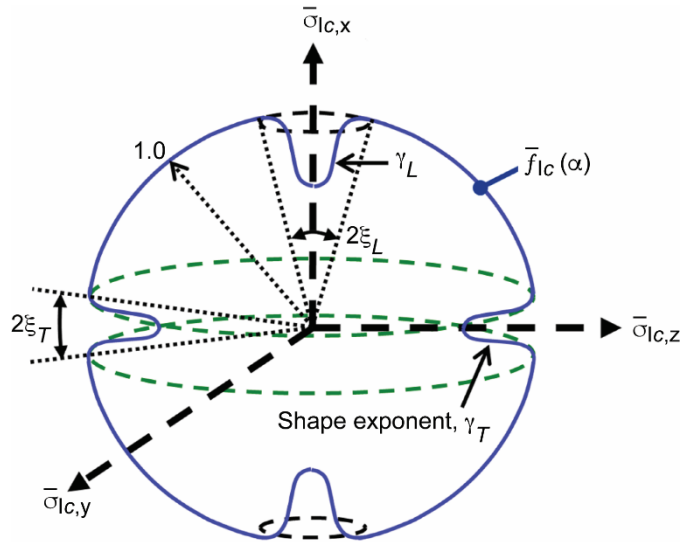
Figure 9.—Anisotropy function $\bar{f}_{Ic}(\alpha)$ in normalized strength space. The *L* subscript correlates with the polar-cap distribution, the *T* subscript correlates with the equatorial-belt distribution, γ is the shape exponent, ξ is an angular width in the critical mode I stress intensity anisotropy function, and $\bar{f}_{Ic}(\alpha)$ is the normalized anisotropy function of the critical mode I stress-intensity factor K_{Ic} or critical mode I strength σ_{Ic}.

3.2.4 Failure Modes

In FEAMAC/CARES a material can have up to five individual failure modes. Material reliability (probability of survival P_s where $P_s = 1 - P_f$) is assumed to be the product of the survival probability of all of the failure modes:

$$P_s = \prod_{i=1}^{n} \left(P_{s,i} \right) \tag{9}$$

where each failure mode (denoted with the subscript *i*) has its own unique failure criterion and parameter description. For example, for an isotropic material volume, two failure modes can be assumed: one for tensile failure and the other for compressive failure. The tensile-failure mode is described by Equation (3) and the compressive-failure mode by Equation (4). The compressive-failure criterion is assumed to be of a different nature than the tensile-failure mode—possibly involving the interaction of arrested cracks (flaws with initial crack growth that subsequently stops because of the angle of the crack growth and the interaction with the local stress field). Regardless, the Weibull distribution is assumed to describe the stochastic strength phenomenologically.

4.0 Example Problems, Performance, and Discussion

This section provides several predictive simulations to illustrate and gauge the performance of FEAMAC/CARES. Most of these example problems rely on simple rectangular-shaped tensile specimen geometry that is modeled using shell elements, although FEAMAC/CARES is not limited to this element type. These problems include the multiaxial response, the longitudinal and transverse stress-strain response, and the "adjusted element" response of a unidirectional ply. Also, an example of SCG degradation is shown. In this report we only examine the response for a unidirectional ply because it is the

simplest and most basic composite system. It provides a good first test illustrating the basic behavior and performance of the FEAMAC/CARES tool. A more involved problem involving a laminated silicon carbide fiber with reaction-bonded silicon nitride matrix in off-axis loading is described in a separate paper (Nemeth et al., 2016).

4.1   Example Problem 1: MAC/GMC Multiaxial Performance of a Polymer Matrix Composite Under Biaxial Loading

In this problem the multiaxial failure response of a unidirectional PMC under biaxial loading was simulated using the GMC technique and the CARES/*Life* unit sphere methodology for strength anisotropy. The PMC experimental results came from the World-Wide-Failure Exercise (WWFE) as reported in Hinton et al. (2004). The WWFE provided a widely used set of benchmark PMC multiaxial testing data with which to compare various composite failure theories. This problem exercise compared results from an RUC generated from MAC/GMC to those of an RUC generated from finite element modeling. The analysis of the multiaxial failure response using the finite element model of the RUC also is reported in Nemeth (2013a, 2014b).

For this problem (and for this report) the analysis was performed with the GMC technique only. Although the HFGMC methodology provides more accurate RUC subcell stress fields, it does so at an order of magnitude greater computational effort. HFGMC should yield results nearly identical to those of Nemeth (2013a, 2014b) for a highly detailed RUC model. Here we desired to see what relative inaccuracy is introduced with the GMC technique in comparison to FEA results. The problem described here was taken from the WWFE (Hinton et al., 2004) of a unidirectional PMC under biaxial tensile loading and was also reported in Nemeth (2013a, 2014b) using the unit sphere methodology for anisotropic strength. In Nemeth (2013a, 2014b) a finite element model of a square-packed fiber-in-matrix RUC with 60-vol% fibers was used. The specimen was loaded under combined longitudinal (parallel to the fiber axis) and transverse (transverse to the fiber axis) loading. The failure response for various variations of the unit sphere model was tested at six highly stressed points in the RUC. The unit sphere model was used as a criterion for failure at the highest stressed point and did not account for the effect of stress gradients and material volume. In the present problem, Equation (5) was used to determine the reliability (and failure probability) of the composite for fiber-tensile, matrix-tensile, and matrix-compressive failure modes, including the effect of stress gradients and material volume.

Figure 10(a) compares the 50-percent probability-of-failure envelopes in stress quadrants I and IV with results from the finite element model (see model M3a in Nemeth, 2013a, 2014b, for details on the model construction) and results generated from MAC/GMC with CARES/*Life* for the RUC shown in Figure 10(b) (analysis of RUC only—without any finite element model of a component) versus the global applied stresses on the composite. The parameters used to generate the plot were chosen so that the longitudinal tensile strength, the transverse tensile strength, and the transverse compressive strength closely matched the reported measured strengths from the WWFE (which we assumed should approximately correlate to 50-percent probability of failure). This is the usual procedure of calibrating a model to experimental data. However, because there were differences in the resolved stress fields between the FEA-generated and MAC/GMC-generated stress fields in the RUC, two different sets of Weibull and anisotropic strength parameters were required to calibrate to the experimental data. This was due to differences between the two different methodologies (MAC/GMC versus FEA) as well as the differences between the fidelity in the resolved stress fields between the two different analytical methods.

This comparison case assumed that there were no residual stresses present in the material constituents and that the volume of the RUC was normalized to a value of 1.0. The unit sphere model with σ_{Ic} strength anisotropy with flaw orientation was used. The MAC/GMC analysis used the functional equivalent to Equation (1) for all subcells in the RUC to obtain the results for a CARES/*Life* calculated probability of failure of 50 percent. No progressive damage analysis was performed, and the 50-percent probability of failure corresponds to the probability of the first damage event occurring under the prescribed level of biaxial loading. The figure shows quite good correlation between the 50-percent probability-of-failure

envelopes generated from the finite element model of the RUC (in Nemeth, 2013a, 2014b) and the results from the analysis of the RUC done with MAC/GMC despite the differences in the two analysis approaches. The Weibull and unit-sphere-specific parameters used to generate the plot are shown in Table I for the MAC/GMC and FEA, respectively.
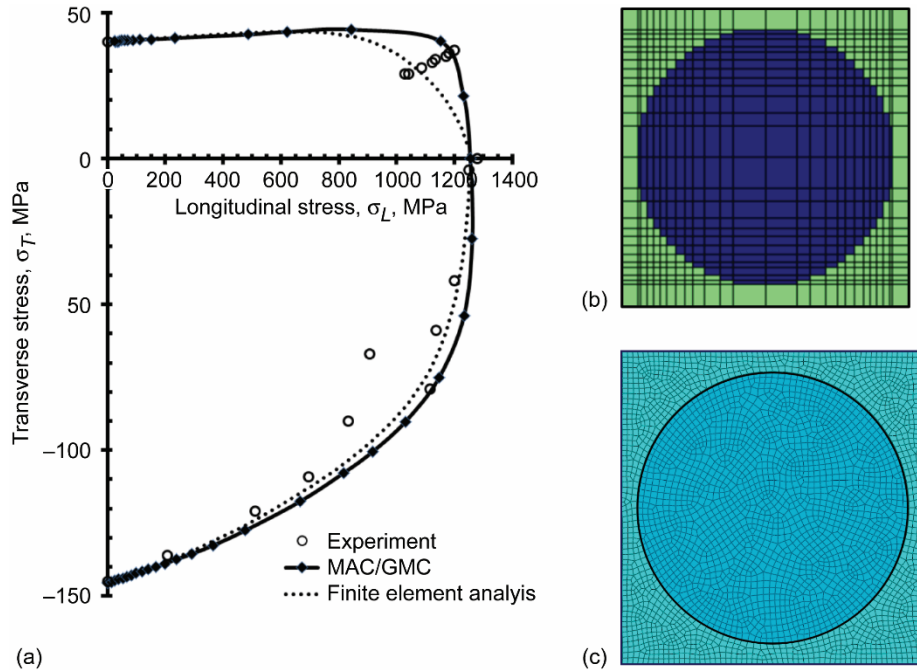

Figure 10.—Example of biaxial response predicted from a MAC/GMC repeating unit cell (RUC) for combined longitudinal L and transverse T loading on a unidirectional polymer matrix composite (PMC). (a) 50-percent probability-of-failure envelope. (b) Schematic of fiber-embedded-in-matrix RUC in MAC/GMC analysis. (c) Finite element mesh of round fiber embedded in matrix from Nemeth (2013a, 2014b).

TABLE I.—PARAMETERS FOR POLYMER MATRIX COMPOSITE (PMC) UNDER BIAXIAL LOADING FOR REPEATING UNIT CELL (RUC) GENERATED BY MAC/GMC AND FINITE ELEMENT ANALYSIS (FEA) FROM NEMETH (2013a, 2014b) WITHOUT RESIDUAL THERMAL STRESSES FROM PROCESSING

RUC generated from	Failure (fiber or matrix): Mode	Model and mode[a]	Weibull modulus, m_V	Characteristic strength, $\sigma_{\theta V}$, MPa	Shetty shear-sensitivity constant, $\overline{C}$	Constant (ratio) or parameter in K_{Ic} anisotropy function, r
MAC/GMC	Fiber: Tensile[b,c]	L flaw Anisotropic	10.0	2036	1.4	-------
	Matrix: Transverse tensile[d]	T critical strength Anisotropic	10.0	109.4	100.0	2.776
	Matrix: Transverse compressive[b]	Isotropic	10.0	119.8	------	-------
FEA	Fiber: Tensile[b,c]	L flaw Anisotropic	10.0	2147	1.4	-------
	Matrix: Transverse tensile[d]	T critical strength Anisotropic	10.0	111.8	1.4	1.776
	Matrix: Compressive[b]	Isotropic	10.0	170.6	------	-------

[a]L, longitudinal; T, transverse.

[b]The constants ξ, γ, and r are not used.

[c]One-half angle of anisotropy distribution, Λ, 1.0°; exponent of sine or cosine function, ϕ, 0.0.

[d]Set for 1500-MPa longitudinal strength at 50-percent probability of failure; one-half angle of anisotropic distribution for critical mode I stress intensity factor, ξ, 10°; exponent of sine or cosine function, γ, 1.0.

Some significant differences in the Table I parameters for the MAC/GMC-generated RUC and the FEA-generated RUC require some explanation. The large differences are due mainly to differences in the peak stresses for the two types of analyses. The difference in using a maximum-stressed-point failure criterion in the FEA of Nemeth (2013a, 2014b) versus the full stress-volume integration (see Eq. (5)) is more of a secondary effect as explained in Nemeth (2013a, 2014b). In Table I the characteristic strength $\sigma_{\theta V}$ (the peak stress in the component at 0.6321 probability of failure, as explained in Nemeth et al., 2003, 2005) for the fiber tensile strength and matrix tensile strength, respectively, are relatively close to one another for the RUCs generated by MAC/GMC and FEA. However, significant differences are seen in the transverse compressive $\sigma_{\theta V}$ of the matrix and in the constant r, which calibrates the relative degree of strength anisotropy. A higher r value correlates with a higher degree of strength anisotropy in the material. The MAC/GMC RUC model required a significantly higher r value to correlate with the experimental data than did the finite element model of the RUC. In fact the larger value of r in the MAC/GMC model necessitated using a large value for the Shetty shear-sensitivity constant $\overline{C}$ (making the material more "shear insensitive") to calibrate the model. However, Nemeth (2013a, 2014b) show that $\overline{C}$ had only a small influence on the multiaxial response for this particular example, so the differences in $\overline{C}$ between the MAC/GMC-generated and FEA-generated RUCs are not very relevant.

The reason for the disparity of parameters is due mainly to the GMC not resolving the highest stresses and stress concentrations as completely as FEA. This is demonstrated in Figure 11, which is reproduced from Aboudi et al. (2013). The figure compares results from FEA, GMC analysis, and HFGMC analysis for a PMC square-packed fiber-in-matrix RUC under a transverse tensile loading. Figure 11 shows the axial stress distribution for the stress component oriented in the same direction as the applied strain (applied left-to-right, which is transverse to the fiber) in the figure. Figure 11(a) shows the stress results from FEA, which are assumed to be the most accurate results. Figure 11(b) shows the results for GMC for a 26×26 subcell RUC, and Figure 11(c) shows results HFGMC for a 32×32 subcell RUC.

What is important to notice is that there is a stress concentration near the fiber on the left- and right-hand side of Figure 11(a) for the FEA results. This stress concentration is reproduced in the HFGMC results in Figure 11(c), but it is underpredicted in the GMC results of Figure 11(b). This is because GMC lacks shear coupling between subcells. The difference shown in peak stress between the FEA and GMC results is significant enough to be the main reason why the r values are different for the matrix tensile strength anisotropy and the matrix characteristic compressive strength $\sigma_{\theta V}$ in Table I. The implications are that a good correlation of multiaxial strength predictions for FEA and MAC/GMC analysis of an RUC can be obtained if the model parameters are adjusted to correlate with experimental material characterization data. However, for the GMC model, the additional parameter adjustments required to calibrate a model can make it less representative of the assumed physical conditions in the RUC.
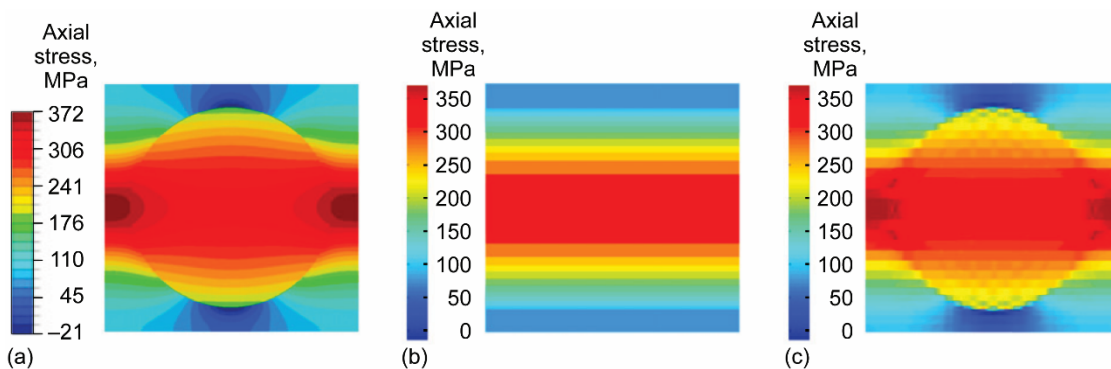

Figure 11.—Comparison of axial stress distributions in a repeating unit cell (RUC) for finite element analysis (FEA) and two MAC/GMC analysis options for a glass/epoxy composite subjected to 0.02 global transverse strain. Axial stress component and strain component are in the same direction—applied left to right in the figure. (a) FEA. (b) MAC/GMC option for a 26×26 RUC. (c) MAC/HFGMC option for a 32×32 RUC. From Figure 6.9 of Aboudi et al. (2013). Copyright © 2013 Elsevier; used with permission.

These results also indicate that the architecture of the RUC—for example, square-packed versus hex-packed, versus random fiber-in-matrix arrangements—will affect the resultant multiaxial stress fields and stress concentrations, particularly when no damage progression is included. A properly calibrated model with reasonably accurate stress fields, nevertheless, seems to be capable of providing good predictive results for applied multiaxial loading. This example problem illustrates some of these issues and suggests that the tradeoffs should be considered early on in an analysis to determine whether the use of HFGMC is necessary.

4.2   Example Problem 2: Effect of Weibull Modulus on Stress-Strain Response of Ceramic Matrix Composite Under Longitudinal Tension

In this example problem, a multiscale simulation was performed to examine the predicted effect of the Weibull modulus m_V on the stress-strain response of a unidirectional CMC under longitudinal tension (along the axis of the fibers). It is known that Weibull modulus affects the stress-strain response, and this has been analytically modeled for a unidirectional composite by Ahn and Curtin (1997). The CMC considered here was based on silicon carbide continuous-fiber-reinforced reaction-bonded silicon nitride matrix (SiC/RBSN), as reported by Bhatt and Phillips (1990) and subsequently analyzed by Goldberg (2012) with MAC/GMC. This material also was used in the companion report to this report (Nemeth et al., 2016), which provides a validation/benchmarking problem for FEAMAC/CARES. It should be noted that there are some differences in the constituent properties and parameters given in these two publications. The analysis performed in Nemeth et al. (2016) is substantially more detailed and involved. Here, we are only illustrating the performance and capability of FEAMAC/CARES and not prioritizing the comparison and benchmarking to experimental data.

We used the same constituent properties as Goldberg (2012), which are listed in Table II. The interface material was a carbon layer with a thickness of 3 percent of the fiber diameter. The fiber volume fraction was taken as 30 percent. The presence of processing-induced residual stresses (from thermal cooldown and thermal expansion mismatch) in the constituents was not considered. Residual stresses in the material constituents can affect the shape of the stress-strain curve, but we only wanted to show how m_V affects the stress-strain response in isolation from residual stresses.

For the FEAMAC/CARES analysis, the gauge section of the rectangular tensile specimen geometry used by Bhatt and Phillips (1990) was modeled with a simple mesh of 10×20 S4-type shell elements (see Fig. 12) for dimensions of 25 by 12.7 by 1.2 mm. A single unidirectional ply was assumed through the specimen thickness, and the RUC architecture shown in Figure 12 was used. This simple 4×4 RUC represents a square fiber in a square-packed unit cell with matrix and interface material present. We used the GMC methodology with an RUC design having a small total number of subcells (16 in this case) for the RUC so that computer memory requirements and problem execution time would not be prohibitive. For the finite element model, appropriate boundary conditions were imposed and a monotonically increasing end displacement over time was applied at the top of the specimen in the direction parallel with the length. The maximum amount of displacement was 0.2 mm for a strain of 0.008, and this was broken into 250 load-step increments. A fast-fracture rupture analysis was performed using the Weibull parameters shown in Table III for the fiber, matrix, and interface. Isotropic strength material constituents were assumed, and the analysis was performed with the unit sphere multiaxial model assuming a penny-shaped crack geometry and a Shetty shear-sensitivity constant of $\bar{C} = 1.0$. The Weibull scale parameter σ_{oV} for the very compliant interface (see Table II) was set to an arbitrarily large value so that initial failure only

TABLE II.—CONSTITUENT PROPERTIES OF SiC/
REACTION-BONDED SILICON NITRIDE (RBSN)

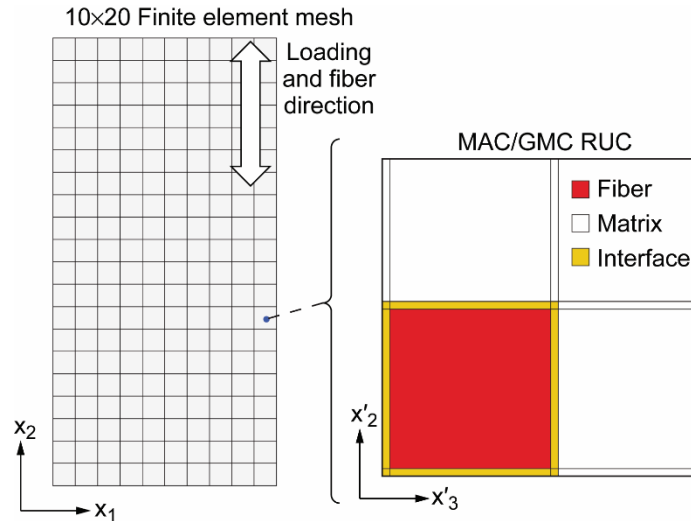| Constituent	Modulus, GPa	Poisson ratio
Fiber	390	0.17
Matrix	110	.22
Interface	1.8	.22

Figure 12.—Finite element model of tensile specimen gauge area and MAC/GMC 4×4 subcell repeating-unit-cell (RUC) architecture used in the problem simulation.

TABLE III.—ASSUMED WEIBULL PARAMETERS FOR EXAMPLE 2

Constituent	Weibull modulus, m_V	Weibull scale parameter, σ_{oV}, MPa • mm$^{3/m_V}$
Fiber	20.0	2875.0
Matrix	5.0 to 60.0	106.0
Interface	5.0 to 60.0	60.0[a]

[a]Large value assigned so that early failure in the interface material is avoided.

occurred in the matrix. Shell element thickness is not available in FEAMAC/CARES, so its effect on volume could only be accounted for indirectly with a volume multiplication factor, which was set to 1.2 for this case. The cellular-automaton feature that adjusted the adjacent element probability of failure was turned on.

Figure 13(a) shows the effect of the value of the matrix and interface Weibull moduli on the stress-strain responses, and Figure 13(b) shows the 10×20 finite element mesh and a damage pattern for a $m_V = 10$ simulation (set as a "quilt" pattern in the Abaqus display options) after significant matrix damage had occurred. Figure 14(a) shows the entire stress-strain curve of a simulation for $m_V = 10$ up to the maximum strain of 0.008, and Figure 14(b) shows the damage pattern at the ultimate failure of the composite. It is clear that there are two distinct damage regions. The first involves failure of the matrix only, and the second involves failure of the fiber and interface.

In Figure 13(a) each curve represents an individual simulation trial. These results vary from trial to trial for a given constant value of Weibull modulus, and more so for the lower Weibull modulus materials because they have increased variability (by definition of what the Weibull modulus represents). This stochastic effect is further demonstrated in Nemeth et al. (2016). The Weibull modulus for the fiber strength distribution was kept constant at 20.0. Because the scale parameter for the fibers was much larger than that for the matrix (see Table III), the early changes in the stress-strain response are attributable to matrix damage only.

In Figure 13(a), the highest considered Weibull modulus ($m_V = 60.0$) has very little scatter in the failure strength of the matrix and interface. In such a case, the composite response appears to be deterministic rather than stochastic. Therefore, the matrix in all element integration points will fail at nearly the same global strain value. When this occurs, there is a sudden loss of stiffness in the whole composite, as indicated by the jog in the curve near 0.00095 strain and 180-MPa stress. Prior to this jog, the stress-strain response is linear with the Young's modulus of the composite E_c as indicated in the figure
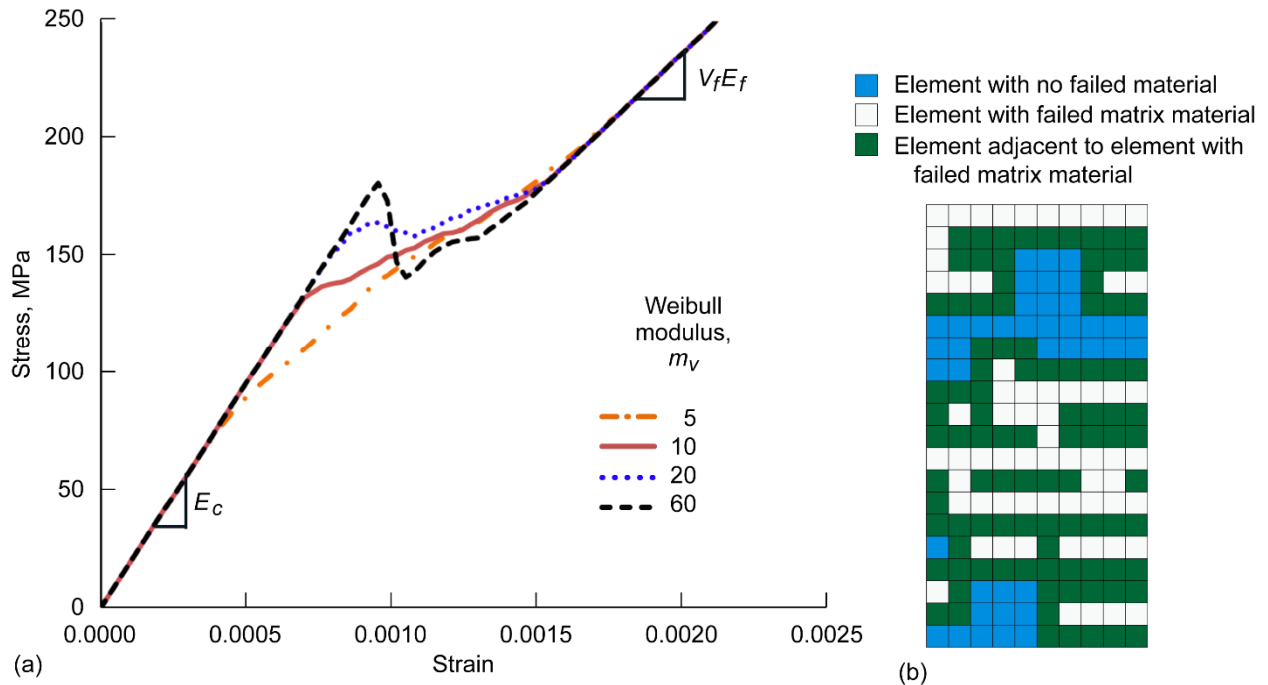
Figure 13.—Simulated global stress-strain response in the matrix cracking region of a unidirectional composite under longitudinal tensile loading. (a) Predicted response for various values of Weibull modulus m_V for the matrix that illustrates the effect of parameter. The composite slope is E_c (Young's modulus of composite), and the fiber-controlled slope is $V_f E_f$ (product of fiber volume fraction of composite and Young's modulus of fibers). (b) The 10×20 finite element mesh used for the model showing a point in time where significant matrix damage had developed in the finite element model (for $m_V = 10$).
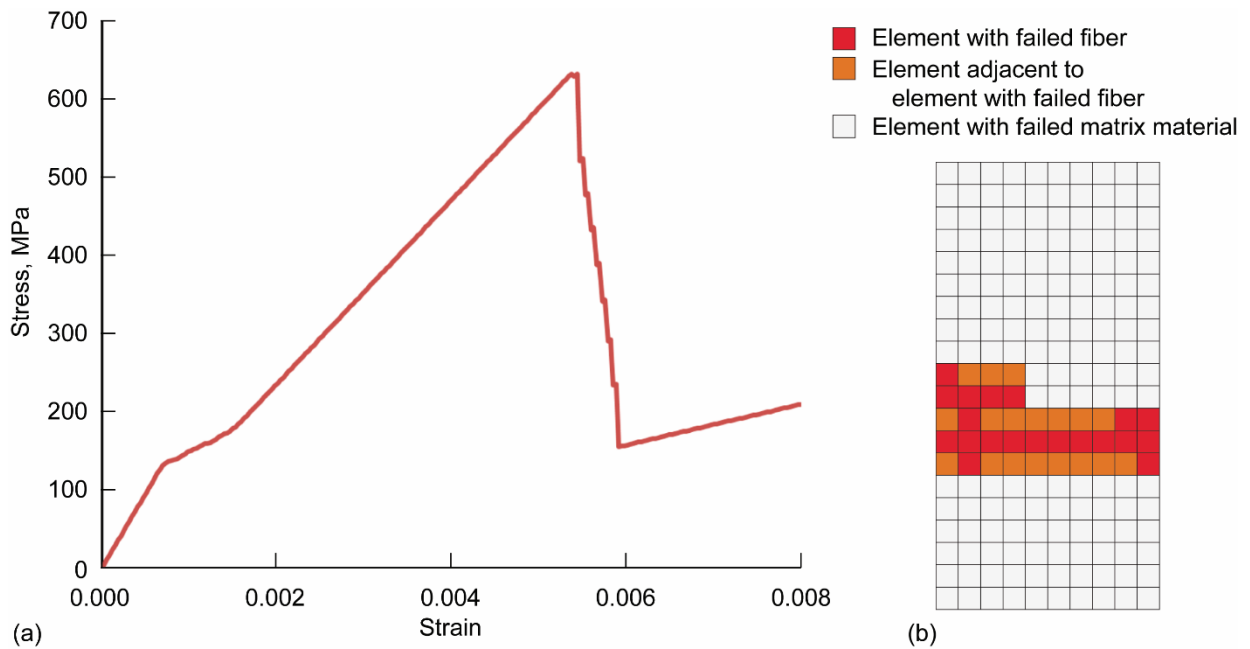

Figure 14.—Entire stress-strain response for Weibull modulus of $m_V = 10$ (from Fig. 13) and fiber failure. (a) Stress-strain curve. (b) The 10×20 mesh showing final fiber failure.

for the undamaged material. Just after the jog, most of the matrix has failed. It took a few additional steps after the main jog for all the matrix and interface material to completely fail (the small hump seen after the main jog). For subsequent loading steps, only the remaining intact fibers controlled the composite response. Initially all the fibers remained intact, and the slope of the line was the Young's modulus of the composite multiplied by the volume fraction of fibers—$V_f E_f$, where V_f is the fiber volume fraction of the composite and E_f is the Young's modulus of the fibers. Figure 14(a) shows a complete stress-strain curve of a simulation run with $m_V = 10$. As the simulation in Figure 14(a) progressed past 0.0054 strain, the fibers failed and the stiffness fell abruptly, indicating that the entire composite had failed. Figure 14(b) shows the elements where final fiber failure occurred.

In an actual CMC, the interface, which is usually weaker than the matrix and the fiber, will be the first material constituent to fail. In that case, failure in the interface may propagate (depending on the conditions) into the matrix causing matrix failure as well. These fracture physics are not considered in the current methodology.

Figure 13(a) shows individual simulations of FEAMAC/CARES for Weibull moduli of 5, 10, and 20. In the curve for $m_V = 20$, the effect of scatter in strength in the matrix material starts to become apparent. This can be seen for the applied strain between 0.0008 and 0.0015, where there is a more gradual transition from the undamaged composite to complete matrix failure, with only the fibers and interface remaining intact. The matrix damage initiation across the composite was more diffused because of the increased scatter in the matrix fast-fracture strength, and it was spread over several time/load steps. This situation is more representative of the actual stress-strain behavior of CMCs: a region of matrix and interface cracking occurs until a saturation point is reached where there is no further damage in these material constituents. Ahn and Curtin (1997) modeled this damage evolution for a unidirectional composite under longitudinally applied tension explicitly from an analytical perspective by considering the Weibull statistics of the matrix and shear-lag behavior. As the Weibull moduli decrease, the curves become more gradual in transitioning from an undamaged state to a fully saturated state of matrix failure. These trends are qualitatively similar to those shown in Ahn and Curtin (1997) and are also representative of actual observed behaviors of CMCs. The Ahn and Curtin (1997) model only applies to a unidirectional ply loaded in longitudinal tension. FEAMAC/CARES does not have this restriction.

4.3   Example Problem 3: Cellular-Automaton Comparison: Damage Response of a Ceramic Matrix Composite Under Longitudinal Versus Transverse Tension

In this problem the predicted damage response of a unidirectional fiber-reinforced CMC specimen separately loaded under longitudinal tension and transverse tension are contrasted. The response with and without the cellular-automaton feature adjusting the adjacent-element failure probabilities is also compared. A unidirectional CMC under longitudinal loading (where tensile loading is applied parallel to the fibers) typically displays nonlinear stress-strain behavior and matrix damage distributed throughout the specimen. At the point where the matrix cracking is fully saturated (the matrix will not damage further with increasing load), the matrix cracks are regularly (periodically) spaced (see Ahn and Curtin, 1997, for example). Conversely, a unidirectional CMC under transverse loading (where tensile loading is applied perpendicular to the fibers and in the plane of the specimen) should only display linear stress-strain behavior until the specimen suddenly and catastrophically fractures from matrix failure into separate pieces. The ability of FEAMAC/CARES to predict these two different fracture behaviors is investigated with this problem.

The modeled CMC material was SiC/RBSN reported from Bhatt and Phillips (1990) (and described in Sec. 4.2), although again the differences between the constituent properties and parameters given here and those in Nemeth et al. (2016) are not significant because here we are only illustrating the performance and capability of FEAMAC/CARES, not prioritizing the comparison and benchmarking to experimental data. The material mechanical properties used are listed in Table II, and the coefficients of thermal expansion are listed in Table IV. An anisotropic thermal expansion coefficient was used for the fiber properties (justified from Saigal et al., 1993), and a cooldown (stress-free) temperature of 550 °C from thermal

TABLE IV.—THERMAL EXPANSION COEFFICIENTS OF SiC/
REACTION-BONDED SILICON NITRIDE (RBSN)

Constituent	Longitudinal coefficient of thermal expansion, α_L, m/m/°C	Transverse coefficient of thermal expansion, α_T, m/m/°C
Fiber	4.1×10^{-6}	1.84×10^{-6}
Matrix	2.2	2.2
Interface	2.0	2.0

TABLE V.—ASSUMED WEIBULL PARAMETERS FOR PROBLEM 3

Constituent	Weibull modulus, m_V	Weibull scale parameter, σ_{oV}, MPa $\bullet$ mm$^{3/m_V}$
Fiber	20.0	2875.0
Matrix	7.0	106.0
Interface	7.0	60.0

processing was assumed. The cooldown step from 550 to 23 °C imparted residual thermal stresses in the material constituents because of their thermal contraction mismatches. This is further explained in Nemeth et al. (2016).

The FEAMAC/CARES analysis modeled the gauge section of a rectangular tensile specimen from Bhatt and Phillips (1990) with a simple mesh of 10×20 S4-type shell elements for specimen dimensions of 25 by 12.7 by 1.2 mm. A single unidirectional ply was modeled using the same RUC architecture shown in Figure 12. For the finite element model, appropriate boundary conditions were imposed and a monotonically increasing displacement over time was applied at the top of the specimen in the direction parallel with the length. A fast-fracture rupture analysis was performed using the Weibull parameters shown in Table V for the fiber, matrix, and interface. Isotropic strength material parameters were assumed, and the analysis was performed with the unit sphere multiaxial model assuming a penny-shaped crack geometry and a Shetty shear-sensitivity constant of $\bar{C} = 1.0$. The Weibull scale parameter σ_{oV} for the interface was set to an arbitrarily large value so that the initial failure would occur only in the matrix. This was done to avoid the situation where the interface failed first but the damage did not propagate into the matrix. Otherwise, initial damage would only have had a minor effect on the RUC stiffness response because the coating has a very low stiffness and was only a small volume fraction of the RUC.

4.3.1 Longitudinal Tensile Loading

Figure 15 shows the predicted stress-strain response for longitudinal tensile loading. The figure shows two simulations: one using the cellular-automaton adjusted-element feature (see Sec. 3.1) and one with the feature turned off. Although there is trial-to-trial variation in the stress-strain response owing to the stochastic nature of the simulation, the results shown in the figure are representative of the typical behaviors. Also shown in the figure is the 50-percent probability of failure of the first matrix cracking event as calculated from CARES/*Life* (Eq. (5)). The probability of a first damage event for each material constituent of the whole composite was calculated at the end of each time step. Figure 16 shows snapshots of the progression of matrix damage for the two simulations.

The number of time steps used in each simulation in Figure 15 was 320, where 10 steps were used for the thermal cooldown, 10 steps largely spanned the initial linear elastic response range of the composite to strain 0.0007, 200 steps largely spanned the matrix damage region between 0.0007 and 0.003 strain, and 100 steps spanned the region of fiber-controlled response from 0.003 to 0.008 strain.
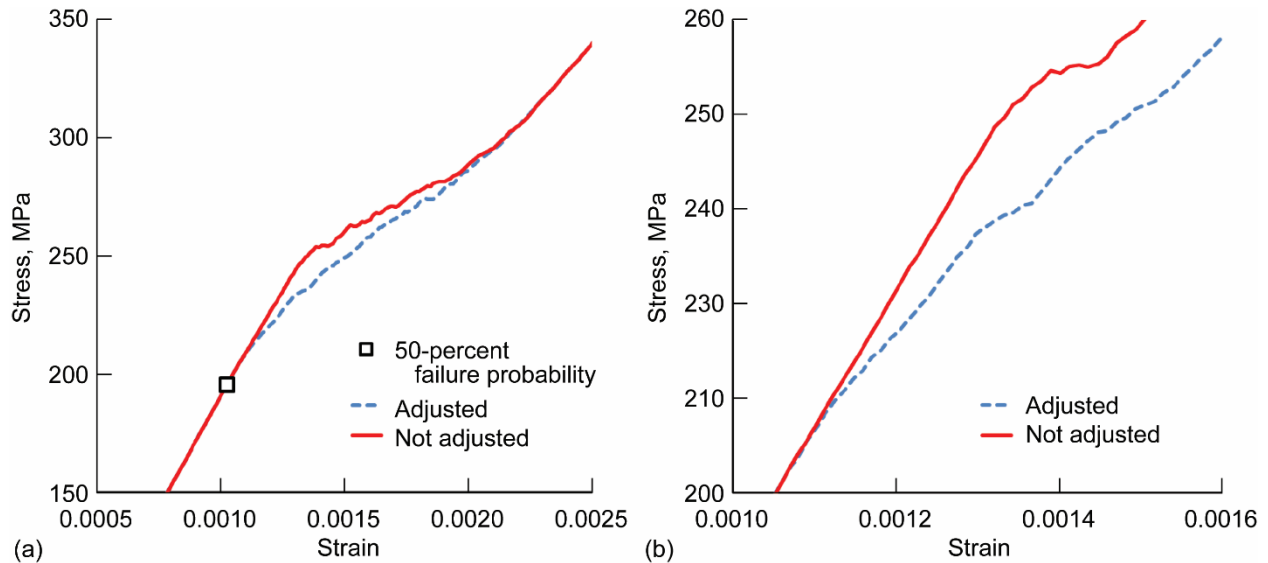
Figure 15.—Predicted stress-strain response of a unidirectional composite loaded in longitudinal tension. Shown are two simulations—one using the cellular-automaton adjusted-element feature and one with the feature turned off. (a) Stress strain response in the matrix cracking region. (b) Closeup of the region where matrix damage initiates.

Figure 15 shows the differences in the stress-strain response with and without the cellular-automaton adjusted-element feature. Figure 15(a) shows the response over the entire matrix cracking region, and Figure 15(b) is a magnified view of the region where matrix damage initiated. The cellular-automaton adjusted-element technique shifted the point of deviation from composite linear-elastic behavior from 240 MPa (when this technique was not used) to a lower stress of approximately 210 MPa. The point where matrix damage becomes fully saturated is about the same for both simulations at approximately 300 MPa.

The reason that the cellular-automaton adjusted-element technique shifted the point of deviation from composite linear-elastic behavior was because the damage was able to localize sooner. This is illustrated in Figure 16, which shows the finite element model of the composite specimen. In Figure 16(a), without this cellular-automaton technique, early matrix damage was diffused throughout the specimen. When there was failure in an element, the subsequent stress redistribution did not cause a high enough stress concentration in the adjacent elements to immediately initiate failure. Because adjacent elements had a higher $P_{f,j(\text{random})}$ (see Fig. 6), they did not fail, even with the stress concentration present. Hence early damage developed in a more diffuse manner, akin to stochastic toughening like that described in Planas (1995) and Bazant and Planas (1998). This also meant that the material resisted the development of damage, taking more time steps to develop the same level of damage than when the cellular-automaton feature was active. Figure 16(d) shows the early development of damage with the cellular-automaton technique active. Here matrix damage has a more organized, localized, and cracklike appearance, with failure tending to progress along a rows of elements. In Figure 16(b), without the automaton technique, the damage developed in a diffuse manner and damage clustering seems to be evident (dashed circles in figure). In contrast, Figure 16(e), with the cellular-automaton feature active, shows a more organized appearance of cracklike damage and less apparent damage clustering. Several rows of failed elements developed, giving a more periodic spacing. Figures 16(c) and (f) show the final failure of the composite. Differences in the element fiber failure pattern between the two figures are less apparent, but the cellular-automaton technique (Fig. 16(f)) does show a more cracklike damage pattern.
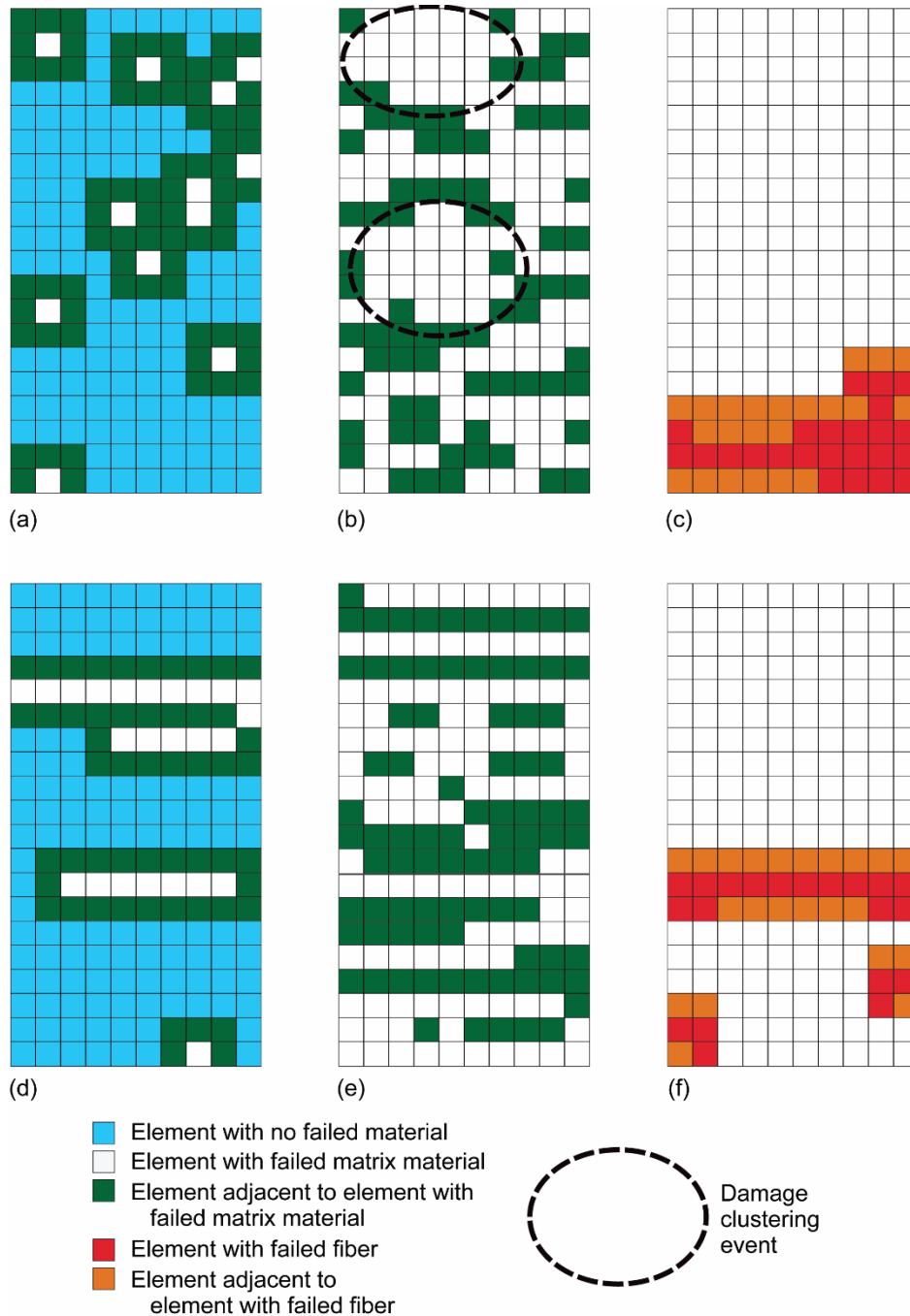
Figure 16.—Progression of damage in the finite element model of a unidirectional ply under longitudinal loading. Loading direction is top to bottom and fibers are aligned parallel to the direction of loading. In (a), (b), and (c), the cellular-automaton adjusted-element feature was turned off; and in (d), (e), and (f), the feature was turned on. Here (a) and (d) show early damage; (b) and (e) show the development of substantial matrix damage; and (c) and (f) show the final failure of the composite (fiber failure).

4.3.2 Transverse Tensile Loading

Figure 17 shows the predicted stress-strain response for transverse tensile loading. The figure shows two simulations: one using the cellular-automaton adjusted-element feature and one with the feature turned off. The results shown are representative of the typical behavior. However, there is substantial simulation-to-simulation variation in the fracture stress, and the CMC behaves more like a monolithic ceramic because the fibers do not bridge the fracture path (the fibers are perpendicular to the load). This stochastic nature is explored further in Nemeth et al. (2016). Also shown in Figure 17(a) is the 50-percent probability of failure of the first matrix cracking event in the specimen as calculated from CARES/*Life* (Eq. (5)). Figure 18 shows snapshots of the progression of matrix damage for the two simulations.

The number of time steps used in each trial in Figure 17 was 220, where 10 steps were used for the thermal cooldown, 10 steps spanned the initial linear elastic response range of the composite until 0.0002 strain, 100 steps spanned the strain region between 0.0002 and 0.0005 strain, and 100 steps spanned the region between 0.0005 and 0.0008 strain. The large number of time steps allowed us to determine the individual trial fracture strength within a reasonably narrow range and to get a detailed look at the development and progression of damage.

Figure 17 shows the differences in the stress-strain response with and without the cellular automaton feature. In both simulations, there is a sudden and large dropoff in stiffness, indicating failure of the matrix. This catastrophic, or brittle-like, failure behavior is consistent with what is observed from specimen rupture experiments of transversely loaded unidirectional CMCs. However, this dropoff is more sudden for the trial using the cellular-automaton adjusted-element technique than for the trial without it. This is evidenced by the slight jaggedness in the line prior to reaching the peak stress ($\approx$34 MPa) and the slower stress dropoff after the peak stress for the trial that did not use the cellular-automaton adjusted-element technique (better seen in Fig. 17(b)). This jaggedness prior to the peak stress is not evident in the trial that used the cellular-automaton adjusted-element technique. The reason for this difference can be understood with Figure 18, which shows the progression of damage in the finite element model of the single-ply specimen.
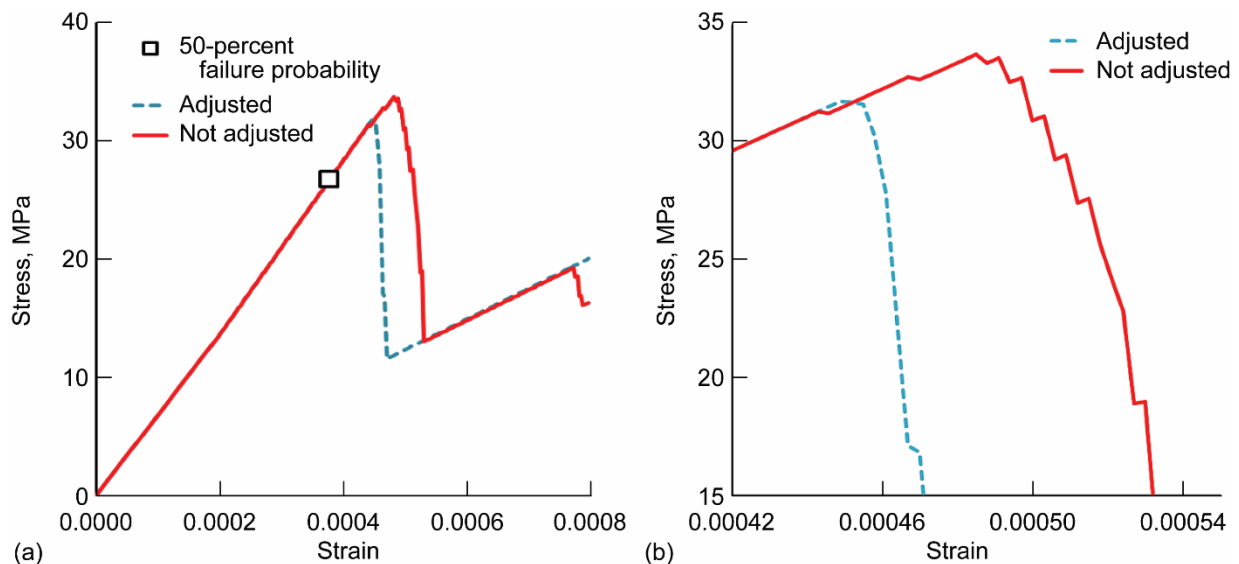

Figure 17.—Predicted stress-strain response of a unidirectional composite loaded in transverse tension. Shown are two trial executions: one using the cellular-automaton adjusted-element feature and one with the feature turned off. (a) Stress-strain response. (b) Closeup of region where matrix cracking occurred.
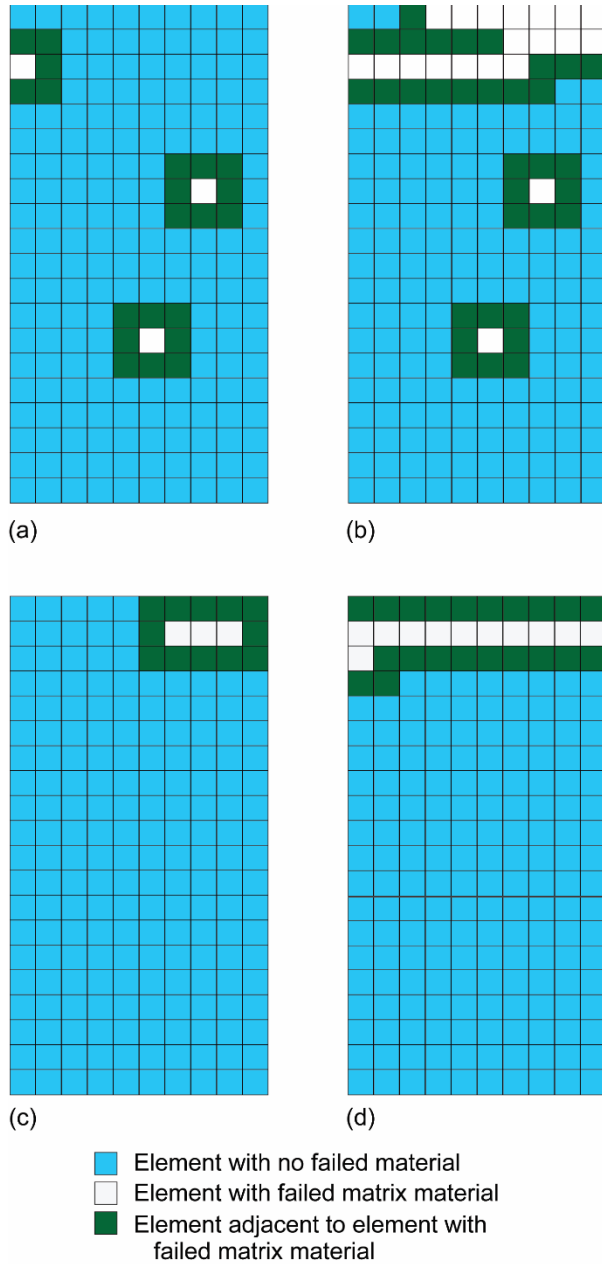
Figure 18.—Progression of damage in the finite element model of a specimen of a unidirectional ply under transverse loading. Loading direction is top to bottom, and the fibers are aligned left to right. In (a) and (b), the cellular-automaton adjusted-element feature is turned off; and in (c) and (d), the feature is turned on. Here (a) and (c) show early damage, and (b) and (d) show the final failure of the composite (from matrix failure).

In Figure 18(a) early damage is more diffused throughout the specimen than in Figure 18(c). When there was failure in an element, the subsequent stress redistribution did not cause a high enough stress concentration in the adjacent elements to immediately initiate failure. The elements adjacent to the failed element had a higher $P_{f,j(\text{random})}$ (see Fig. 6) and did not fail, even with the stress concentration present. Hence early damage developed in a more diffuse manner, again akin to stochastic toughening like that described in Planas (1995) and Bazant and Planas (1998). This behavior is contrary to the brittle-like fracture failure mode typically observed in rupture experiments with transversely loaded unidirectional composites. Instead, it meant that the material resisted the localization of damage. Figure 18(c) shows the early development of damage with the cellular automaton technique. In comparison to Figure 18(a), the damage in Figure 18(c) appears to be more organized and cracklike, with failure localized along a row of elements. Figures 18(b) and (d) show this progression of damage through subsequent time steps until final failure of the composite. Figure 18(d) shows a single cracklike path to failure as would be expected. Figure 18(b) shows a more diffused and distributed damage pattern contrary to what is typically observed in experiments. Clearly Figures 18(c) and (d), which show results with the cellular automaton technique, better represent the physical behavior of fracture of a unidirectional composite under transverse tensile loading. It should be noted that if FEAMAC/CARES used subcell-by-subcell failure instead of failing a whole material in a RUC, the stress-strain response would be more sensitive to the arrangement of the subcells and to the total number of subcells used to model the RUC.

4.4 Example Problem 4: Unidirectional Ceramic Matrix Composite Under Constant Static Loading With Slow Crack Growth

In this example problem the predicted effect of SCG on the time to damage onset is demonstrated for an applied static (nonvarying) load. This example is not correlated with any experimental SCG data but is provided to show how the SCG power law (Eq. (6)) and transient reliability analysis (see Nemeth et al., 2005) operate and can be used to predict component integrity. Effects from cyclic loading were not predicted (see Eq. (7)). It is known that micromechanical mechanisms play a role in the cyclic fatigue degradation response of CMCs. These effects are not considered here, although they are important. That will have to be saved for future work. A good review of these mechanisms can be found in Volume 4, "Fatigue in Ceramic Matrix Composites," by Ramamurty et al. (2000) of the composite material reference work series edited by Kelly and Zweben (2000).

This problem considers a single-ply unidirectional CMC under longitudinal static tensile loading (load applied parallel to the fibers). The modeled CMC material was the SiC/RBSN reported from Bhatt and Phillips (1990) with the material properties listed in Tables II and IV. In problem 4, the same speci-men geometry, finite element model, MAC/GMC RUC, and cooldown load step used for problem 3 (550 °C, the assumed stress-free temperature, to 23 °C) were used to impart residual stresses in the material constituents. Afterward, a static (nonvarying) load over time was applied (an applied force). The temperature was held constant (23 °C), and we assumed that no creep had occurred over that time (MAC/GMC can model the creep response of material constituents).

The applied constant load over time was broken down into several load cases in Abaqus. This was designed so that each order-of-magnitude of time would have 10 time increments. For example, load case 1 applied a static force for 1000 sec with a time increment of 100 sec so that 10 time increments spanned that load case. Load case 2 subsequently applied a static force for 10 000 sec with a time increment of 1000 sec so that 10 time increments spanned that load case. Load case 3 subsequently applied a static force for 100 000 sec with a time increment of 10 000 sec so that 10 time increments also spanned that load case. These load cases were applied sequentially over several orders of magnitudes of time (from lower to higher orders of magnitude of time). The effect of the load cases was cumulative, meaning the effect of the previous load cases was added to the current load case. When damage began to occur, it could evolve further before the next order-of-magnitude time range was encountered.

A power law SCG rupture analysis was performed using the Weibull and SCG parameters shown in Table VI for the fiber, matrix, and interface. The parameters were chosen so that only the matrix material would fail. This was done by making the SCG exponent N_V a large value (100.0) for the fiber and interface so very little SCG could occur over time. The SCG constant B_V was also made arbitrarily large (10^{10} MPa^2•sec). A smaller value of the SCG exponent, $N_V = 20$, was assumed for the matrix material. This value provides substantial SCG with time. The SCG constant B_V was also made smaller (10^9 MPa^2•sec) for the matrix. Isotropic strength material constituents were assumed, and the analysis was performed with the unit-sphere multiaxial model assuming a penny-shaped crack geometry and a Shetty shear-sensitivity constant of $\overline{C} = 1.0$. The cellular automaton feature was activated.

Figure 19 shows the strain response for an applied constant static tensile load over time. Shown are individual simulations at applied stresses of 170, 180, 190, and 200 MPa as well as the CARES/*Life*-calculated 50-percent probability of failure for the matrix material of the specimen at a given load level (prior to any damage initiation in a simulation). There are six trial simulations at each applied level of load.

TABLE VI.—WEIBULL AND SLOW CRACK GROWTH PARAMETERS FOR PROBLEM 4

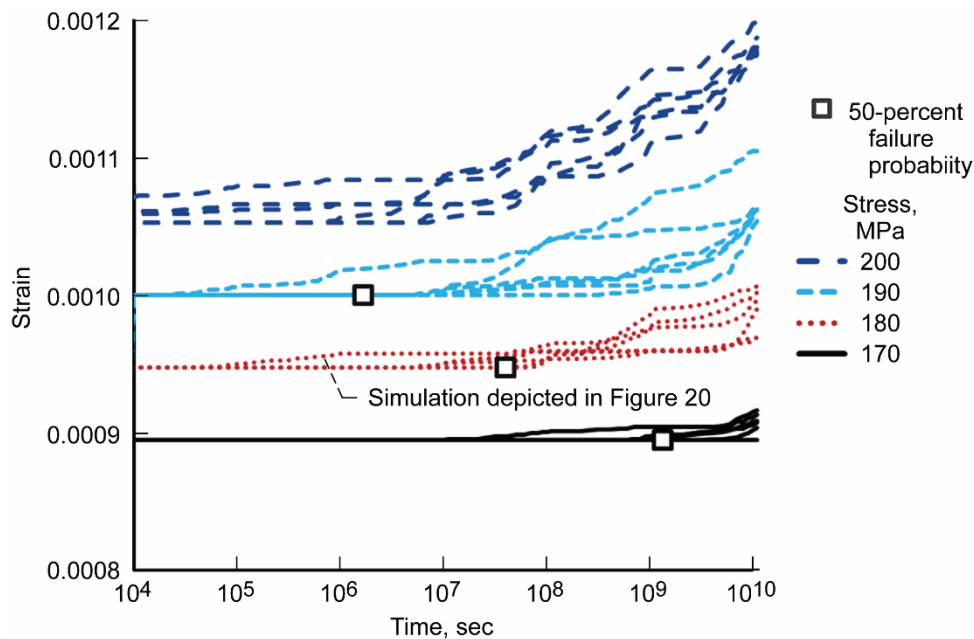| Constituent	Weibull modulus, m_V	Weibull scale parameter, σ_{oV}, MPa•mm$^{3/m_V}$	Fatigue exponent, N_V (Eq. (11))	Fatigue constant, B_V, MPa^2•sec (Eq. (17))
Fiber	20.0	2875.0	100.0	1.0×10^{10}
Matrix	7.0	106.0	20.0	1.0×10^{9}
Interface	7.0	60.0	100.0	1.0×10^{10}

Figure 19.—Strain response for an applied static tensile load over time. Shown are individual simulation trials at applied stresses of 170, 180, 190, and 200 MPa as well as the CARES/*Life*-calculated 50-percent probability of failure for the matrix at a given load level.

The overall trend indicates that when the applied load is decreased, the time when damage becomes evident (where the strain response deviates from the horizontal line) increases. This is as expected. The CARES/*Life*-calculated 50-percent-probability-of-failure data points show this trend more clearly. For the 200-MPa static load, a 50-percent-probability-of-failure data point is not shown because the fast-fracture (at time $t = 0$) probability of failure is already above 50 percent (this is also indicated in Fig. 15(a)). The individual simulations for a given load level show the considerable variability in response that can occur. Of note is that some of the simulations indicate damage initiation at much earlier times than other trials. This can be attributed to the substantial contribution of the fast-fracture strength to the overall probability of failure at earlier times and higher loads. For example, at a time of 10^4 sec and a load of 170 MPa this failure probability is around 4 percent, at 180 MPa it is about 13 percent, at 190 MPa it is about 33 percent, and at 200 MPa it is about 63 percent. This means that, for any given trial, there is reasonable chance that damage will initiate very early and that this chance will increase with increasing applied load.

Figure 20 shows matrix damage progression at an applied stress of 180 MPa for the simulation indicated in Figure 19 with the earliest onset of damage at that load level. Figure 19 shows that after the initial damage there is a long plateau between $\approx 10^6$ and $\approx 4.0 \times 10^9$ sec. Figure 20(a) shows the earliest onset of matrix damage at 4.0×10^4 sec. The cellular automaton technique causes this damage to propagate across the specimen width until 9.0×10^5 sec (Fig. 20(b)). There was no additional damage up to 3.0×10^7 sec and the curve is plateaued in this time region in Figure 19. At 4.0×10^7 sec, a small additional damage occurred at the specimen edges. No additional damage occurred until 4.0×10^9 sec (Fig. 20(d)). Afterward, damage developed rapidly until the end of the trial at 10^{10} sec (Fig. 20(e)).

Figure 19 also shows other noteworthy trends. There is significant scatter in the curves from one trial to the next for a given level of applied load. This reflects the stochastic nature of the matrix strength. The curves often indicate that damage initially develops slowly followed by more rapid damage accumulation, as occurred in Figure 20. The scatter band (for time) for a given level of applied stress tended to decrease as the amount of damage increased.

(a)   (b)   (c)   (d)   (e)

☐ Element with no failed material
☐ Element with failed matrix material
☐ Element adjacent to element with
   failed matrix material

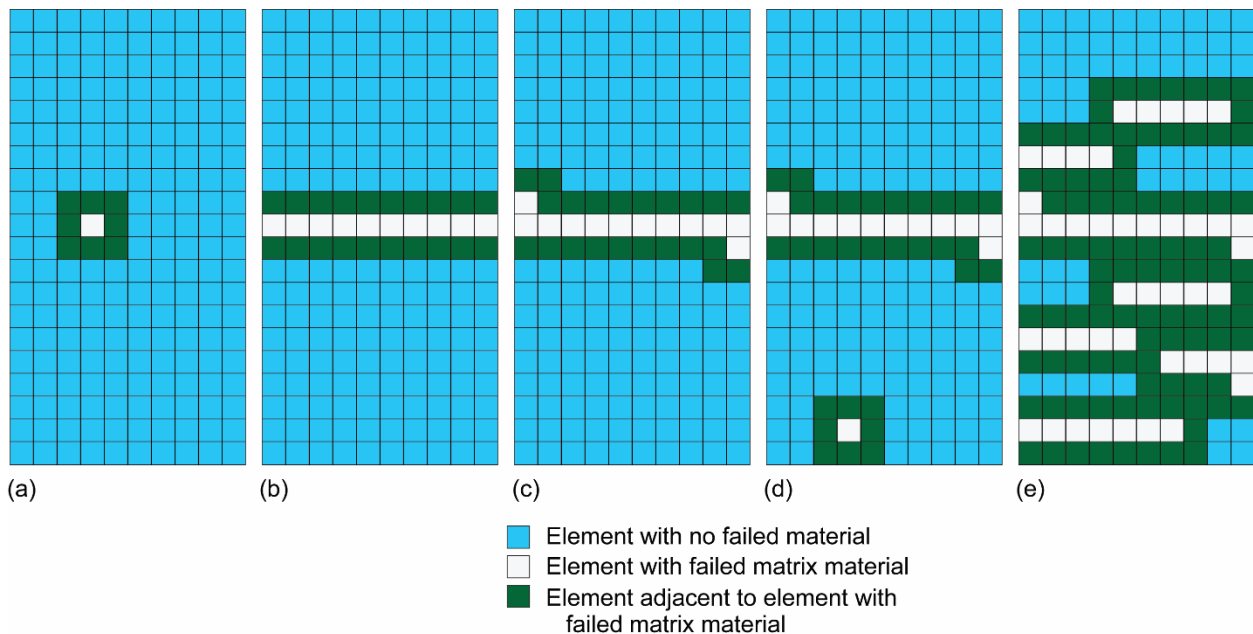Figure 20.—Damage pattern in the matrix for 180-MPa stress applied over time. This trial is indicated by the arrow in Figure 19. (a) Damage initiates at 4.0×10^4 sec. (b) Damage developed at 9.0×10^5 sec and unchanged until 3.0×10^7 sec. (c) Damage developed at 4.0×10^7 sec and unchanged until 3.0×10^9. (d) Damage at 4.0×10^9 sec. (e) Damage at 10^{10} sec.

4.5   Finite Element Mesh, Time Step Sensitivity, and Damage Localization

FEAMAC/CARES simulations are sensitive to the density of the finite element mesh and/or to the number of time steps used per interval of time. This problem is also relevant to the issue of damage localization. It is important to have high mesh density at regions where stress concentration occurs. This is because FEAMAC/CARES treats damage in a step-function manner of complete localized failure. The failure path in these regions should have a cracklike appearance, which means elements should have a small size relative to the size of the stress-concentration feature. The problems shown herein were run using a laptop computer with an Intel I7 generation central processing unit (CPU) with 32 GB of RAM memory. Run times varied with problem complexity. A simulation such as shown in Figure 14 for a fast-fracture analysis would complete in several hours, whereas an SCG time- and load-history-dependent simulation, such as that shown in Figure 19, would take several days.

5.0   Conclusions

This report describes the Finite Element Analysis—Micromechanics Analysis Code/Ceramics Analysis and Reliability Evaluation of Structures (FEAMAC/CARES) multiscale, stochastic, composite modeling tool and its underlying methodology with regard to predicting the durability and life of fiber-reinforced composite components. FEAMAC/CARES is a software tool to simulate stochastic-based discrete-event progressive damage of ceramic-matrix and polymer-matrix composite material structures. This work involved coupling three independently developed software programs: (1) the Micromechanics Analysis Code with Generalized Method of Cells (MAC/GMC), (2) the Ceramics Analysis and Reliability Evaluation of Structures Life Prediction Program (CARES/*Life*), and (3) the Abaqus finite element analysis (FEA) program. MAC/GMC contributes multiscale modeling capabilities and micromechanics relations to determine stresses and deformations at the microscale of the composite material repeating unit cell (RUC). CARES/*Life* contributes statistical multiaxial failure criteria that can be applied to the individual brittle-material constituents of the RUC. Abaqus is used to model the overall composite structure. An Abaqus user-defined material (UMAT) was developed that enables MAC/GMC and CARES/*Life* to operate interactively with the Abaqus FEA code. For each FEAMAC/CARES simulation trial, the stochastic nature of brittle material strength results in random discrete damage events that incrementally progress and lead to ultimate structural failure.

The problems that were examined only involved unidirectional composites. The follow-on paper will expand on this to examine composite laminates under off-axis loading. The problems that were presented here follow:

(1) Multiaxial response of a polymer matrix composite under biaxial loading using the unit sphere failure criterion and MAC/GMC RUC architecture of a fiber embedded in a matrix.
(2) Stress-strain response of a longitudinally loaded unidirectional ceramic matrix composite (CMC) tensile specimen as a function of the Weibull scatter parameter of the matrix.
(3) Stress-strain response of a longitudinally loaded and transversely loaded unidirectional CMC tensile specimen contrasting the failure response for these different loading configurations while examining the response of the cellular-automaton adjusted-element technique.
(4) Demonstrating the predicted slow-crack-growth damage response of a longitudinally loaded unidirectional CMC tensile specimen as a function of static applied load over time.

These problems, involving simple component geometries, served to establish the baseline performance of FEAMAC/CARES with regard to composite failure. FEAMAC/CARES attempts to predict the stochastic nature and mechanisms of failure for the onset and propagation of damage. It provides useful information such as probability of initiation of damage, whether a composite's failure response is brittle-like or shows more graceful failure, and whether scatter is significant in the failure response or not. FEAMAC/CARES can enable faster execution times of multiscale problems because of

the MAC/GMC micromechanics modeling approach, which allows for a tradeoff between solution fidelity and speed of execution.

The combination of knowing the stochastic behavior, stress-strain response, and probability of initial damage provides several important pieces of information with regard to predicting the durability and life of composites. That, plus the generalized nature of FEAMAC/CARES enables the modeling of components for different composite architectures under complex thermomechanical loading. We believe that this provides a good foundation with which to include improved physical models of composite failure at the micro level of the RUC as well as additional models that consider the stochastic creep response and environmental degradation.

Appendix—Symbols

A	area, also power law slow-crack-growth constant
A_1, A_2	crack-growth constants
a	crack length
$B_{V,k}$	fatigue constant at time step k
$\overline{C}$	Shetty shear-sensitivity coefficient
E_c	Young's modulus of the composite
E_f	Young's modulus of the fiber
f_c	cyclic loading frequency
$\overline{f}_{Ic}$	normalized function expressing the degree of mode I anisotropy
g	constant related to the shape of the cyclic loading waveform
h	height
i	integer value; i^{th} subcell; i^{th} link; i^{th} time step; i^{th} failure mode
j	integer value; j^{th} material; element integration point
K_{Ic}	mode I stress intensity factor or fracture toughness
K_{Ieq}	equivalent or effective mode I stress intensity factor
$K_{Ieq,max}$	maximum value of K_{Ieq} in the cyclic loading waveform
$K_{Ieqc,k}$	critical equivalent mode I stress-intensity factor from applied multiaxial stress at step k
k	time step number
$\overline{k}_{BV}$	normalized Batdorf crack-density coefficient
L	longitudinal distribution of flaw
l	length
n	integer value; number of subcells; number of links; normal
m_V	Weibull modulus for volume-based analysis
N	crack-growth-constant exponential term
N_V	volume-flaw crack-growth-constant exponential term
$N_{V,k}$	volume-flaw crack-growth-constant exponential term at time step k
P_f	probability of failure
$P_{fj(CARES)}$	CARES-generated probability of failure or damage initiation probability for repeating unit cell (RUC) for material j
$P_{f,j(random)}$	random-number-generated probability of failure or damage initiation probability for repeating unit cell (RUC) for material j
ΔP_{fV}	incremental failure probability
P_s	probability of survival
Q	Walker fatigue law R-ratio sensitivity exponent
R	ratio of minimum to maximum stress in a cycle
r	constant describing the relative degree of anisotropy of σ_{Ic} versus orientation
ROR	risk of rupture
T	transverse distribution of flaw
t	time
V	volume

V_e	effective volume
V_f	fiber volume fraction of the composite
x,y,z	point location in the structure
Y	crack geometry correction factor or shape factor
α, β	angular orientation coordinates (see Fig. 7)
α_L, α_T	longitudinal and transverse coefficients of thermal expansion
γ_L, γ_T	constants or parameters in K_{Ic} anisotropy function (exponent of sine or cosine function) representing the longitudinal (L, polar-cap) distribution and transverse (T, equatorial-belt) distribution
Λ_L, Λ_T	constants or parameters in flaw-orientation anisotropy function (one-half angle of anisotropy distribution) representing the longitudinal (L, polar-cap) distribution and transverse (T, equatorial-belt) distribution
ν	Poisson's ratio
ξ_L, ξ_T	constants or parameters in K_{Ic} anisotropy function (one-half angle of anisotropic distribution for critical mode I stress intensity factor) representing the longitudinal (L, polar-cap) distribution and transverse (T, equatorial-belt) distribution
σ	applied stress
σ_c	critical strength of a flaw
σ_{cr}	critical strength of a flaw associated with a random number
σ_{Ic}	mode I critical strength
σ_{Ieqc}	equivalent mode I critical strength
$\sigma_{Ic,max}$	maximum value of σ_{Ic} over the unit sphere (for all α and β)
σ_{Ieq}	effective or equivalent stress
σ_n	stress normal to a crack plane
σ_o	Weibull scale parameter
σ_{oV}	Weibull scale parameter normalized to volume
$\sigma_{\theta V}$	Weibull characteristic strength for intrinsic volume flaws
$\sigma_x, \sigma_y, \sigma_z$	stress components parallel to the x, y, z axes
$\overline{\sigma}_{Ic,x}, \overline{\sigma}_{Ic,y}, \overline{\sigma}_{Ic,z}$	orthogonal critical strength components normalized by $\sigma_{Ic,max}$
ϕ_L, ϕ_T	constants or parameters in flaw-orientation anisotropy function (exponent of sine or cosine function) or in K_{Ic} anisotropy function representing the longitudinal (L, polar-cap) distribution and transverse (T, equatorial-belt) distribution.
τ	shear stress acting on a crack plane
Π	multiplication product
Σ	summation, also multiaxial stress state

References

Aboudi, J.; Arnold, S.M.; and Bednarcyk, B.A., 2013: Micromechanics of Composite Materials: A Generalized Multiscale Analysis Approach. Elsevier, Oxford, UK.

Ahn, B.K.; and Curtin, W.A., 1997: Strain and Hysteresis by Stochastic Matrix Cracking in Ceramic Matrix Composites. J. Mech. Phys. Solids, vol. 45, no. 2, pp. 177–209.

Batdorf, S.B., 1978: Fracture Statistics of Polyaxial Stress States. Fracture Mechanics, Nicholas Perrone et al., eds., University Press of Virginia, Charlottesville, VA, pp. 579−592.

Batdorf, S.B.; and Crose, J.G., 1974: A Statistical-Theory for the Fracture of Brittle Structures Subjected to Nonuniform Polyaxial Stresses. J. Appl. Mech. Trans. ASME, vol. 41, no. 2, 1974, pp. 459–464.

Batdorf, S.B.; and Heinisch, H.L., 1978: Weakest Link Theory Reformulated for Arbitrary Fracture Criterion. J. Am. Ceram. Soc., vol. 61, nos. 7−8, 1978, pp. 355−358.

Bazant, Zdenek P.; and Planas, Jaime, 1998: Fracture and Size Effect in Concrete and Other Quasibrittle Materials. CRC Press, Boca Raton, FL.

Bednarcyk, Brett A.; and Arnold, Steven M., 2002a: MAC/GMC 4.0 User's Manual—Keywords Manual. NASA/TM—2002-212077/VOL2. http://ntrs.nasa.gov

Bednarcyk, Brett A.; and Arnold, Steven M., 2002b: MAC/GMC 4.0 User's Manual—Example Problem Manual. NASA/TM—2002-212077/VOL3. http://ntrs.nasa.gov

Bednarcyk, Brett A.; and Arnold, Steven M., 2006: A Framework for Performing Multiscale Stochastic Progressive Failure Analysis of Composite Structures. Proceedings of the 2006 ABAQUS Users' Conference, Cambridge, MA.

Bhatt, R.T.; and Phillips, R.E., 1990: Laminate Behavior for SiC Fiber-Reinforced Reaction-Bonded Silicon Nitride Matrix Composites. J. Compos. Tech. Res., vol. 12, no. 1, pp. 13–23.

Brueckner-Foit, A., et al., 2000: Limitations of the Weibull Theory in Stress Fields With Pronounced Stress Gradients. ASME Paper 2000–GT–0663.

Connecticut Reserve Technologies, Inc., 2015: CARES Version 9.4. Gates Mills, Ohio. http://www.CeramicReliability.com Accessed June 28, 2016.

Curtin, W.A., 1991: Fiber Fragmentation in a Single-Filament Composite. Appl. Phys. Lett., vol. 58, no. 11, pp. 1155–1157.

Curtin, W.A., 1993: Multiple Matrix Cracking in Brittle Matrix Composites. Acta Metall. Mater., vol. 41, no. 5, pp. 1369–1377.

Curtin, W.A., 2000: 4.03—Stress-Strain Behavior of Brittle Matrix Composites. Comprehensive Composite Materials, Anthony Kelly and Carl Zweben, eds., Vol. 4, Elsevier Ltd., New York, pp. 47–76.

Dassault Systemes Simulia Corp., 2011: Abaqus Analysis User's Manual. Version 6.11-1.

Evans, A.G., 1995: Ceramics and Ceramic Composites as High-Temperature Structural Materials: Challenges and Opportunities. Phil. Trans. R. Soc. A, vol. 351, no. 1697, 1995, pp. 511–527.

Goldberg, Robert K., 2012: Utilization of the Generalized Method of Cells to Analyze the Deformation Response of Laminated Ceramic Matrix Composites. NASA/TM—2012-217737. http://ntrs.nasa.gov

Guillaumat, L.; and Lamon, J., 1996: Probabilistic-Statistical Simulation of the Non-Linear Mechanical Behavior of a Woven SiC/SiC Composite. Compos. Sci. Technol., vol. 56, pp. 803–808.

Hinton, M.J.; Kaddour, A.S.; and Soden, P.D., 2004: Failure Criteria in Fibre-Reinforced-Polymer Composites. Sec. 1, Elsevier Ltd., New York.

Iarve, Endel V., et al., 2011: Mesh-Independent Matrix Cracking and Delamination Modeling in Laminated Composites. Int. J. Numer. Meth. Eng., vol. 88, no. 8, pp. 749–773.

Kelly, Anthony; and Zweben, Carl, eds., 2000: Comprehensive Composite Materials, Elsevier Ltd., New York.

Lamon, J.; Thommeret, B.; and Percevault, C., 1998: Probabilistic-Statistical Approach to Matrix Damage and Stress-Strain Behavior of 2–D Woven SiC/SiC Ceramic Matrix Composites. J. Eur. Ceram. Soc., vol. 18, pp. 1797–1808.

Lutz, Gunther, 2006: The Puck Theory of Failure in Laminates in the Context of the New Guideline VDI 2014 Part 3. Proceedings of a Conference on Damage in Composite Materials 2006, Stuttgart, Germany.

Miller, Robert J., et al., 2006: Durability and Life Prediction of Ceramic Matrix Composites (CMC). AFRL–ML–WP–TR–2006–4101,V2.

Nemeth, Noel N., et al., 2003: CARES/LIFE Ceramics Analysis and Reliability Evaluation of Structures Life Prediction Program. NASA/TM—2003-106316, 2003. http://ntrs.nasa.gov

Nemeth, Noel N.; Jadaan, Osama M.; and Gyekenyesi, John P., 2005: Lifetime Reliability Prediction of Ceramic Structures Under Transient Thermomechanical Loads. NASA/TP—2005-212505. http://ntrs.nasa.gov/

Nemeth, Noel N., 2013a: Unit-Sphere Multiaxial Stochastic-Strength Model Applied to Anisotropic and Composite Materials. NASA/TP—2013-217749. http://ntrs.nasa.gov/

Nemeth, Noel, 2013b: Unit-Sphere Anisotropic Multiaxial Stochastic-Strength Model Probability Density Distribution for the Orientation of Critical Flaws. NASA/TM—2013-217810, 2013. http://ntrs.nasa.gov/

Nemeth, Noel N., 2014a: Probability Density Distribution of the Orientation of Strength-Controlling Flaws From Multiaxial Loading Using the Unit-Sphere Stochastic Strength Model for Anisotropy. Int. J. Fracture, vol. 185, nos. 1–2, pp. 97–114.

Nemeth, Noel N., 2014b: Unit-Sphere Multiaxial Stochastic-Strength Model Applied to a Composite Material. J. Compos. Mater., vol. 48, no. 27, pp. 3395–3424.

Nemeth, Noel, et al., 2016: Stochastic-Strength-Based Damage Simulation of Ceramic Matrix Composite Laminates. NASA/TM—2016-219115.

Planas, J., 1995: Crack Growth in an Elastic Medium With Random Crack Growth Resistance. Report No. 95-jp03, Departamento de Ciencia de Materiales, ETS de Ingenieros de Caminos, Universidad Politecnica de Madrid, Ciudad Universitaria sn. 28040 Madrid, Spain, 1995.

Paley, M., and Aboudi, M., 1992: Micromechanical Analysis of Composites by the Generalized Method of Cells. Mech. Mat., vol. 14, no. 2, pp. 127–139.

Pineda, Evan J., et al., 2009: Multiscale Failure Analysis of Laminated Composite Panels Subjected to Blast Loading Using FEAMAC/Explicit. NASA/TM—2009-215813.

Rahman, Sharif; Nemeth, Noel N.; and Gyekenyesi, John P., 1998: Life Prediction and Reliability Analysis of Ceramic Structures Under Combined Static and Cyclic Fatigue. ASME Paper 98−GT−569.

Ramamurty, U.; McNulty, J.C.; and Steen, M., 2000: 4.07—Fatigue in Ceramic Matrix Composites. Comprehensive Composite Materials, Anthony Kelly and Carl Zweben, eds., Elsevier Ltd., New York.

Saigal, A., et al., 1993: Thermal Residual Strains and Stresses in Silicon Carbide-Fiber-Reinforced Silicon Nitride Composites. Compos. Eng., vol. 3, no. 11, pp. 1075–1086.

Shetty, D.K., 1987: Mixed-Mode Fracture Criteria for Reliability Analysis and Design With Structural Ceramics. J. Eng. Gas Turbines Power, vol. 109, no. 3, pp. 282–289.

Sullivan, Rani W.; and Arnold, Steven M., 2011: An Annotative Review of Multiscale Modeling and Its Application to Scales Inherent in the Field of ICME. Models, Databases, and Simulation Tools Needed for the Realization of Integrated Computational Materials Engineering. ASM International, Materials Park, OH, pp. 6–23.

Weibull, W., 1939a: A Statistical Theory of the Strength of Materials. Ingeniorsvetenskapsakademiens Handlingar, no. 151.

Weibull, W., 1939b: The Phenomenon of Rupture in Solids. Ingeniorsvetenskapsakademiens Handlingar, no. 153.